THERMOPHOTOVOLTAIC SPACE POWER SYSTEM

PHASE 3 FINAL REPORT
NAS8 33436

Submitted February 1987

to

NASA Marshall Space Flight Ctr

MARSHALL SPACE FLIGHT CENTER, ALABAMA

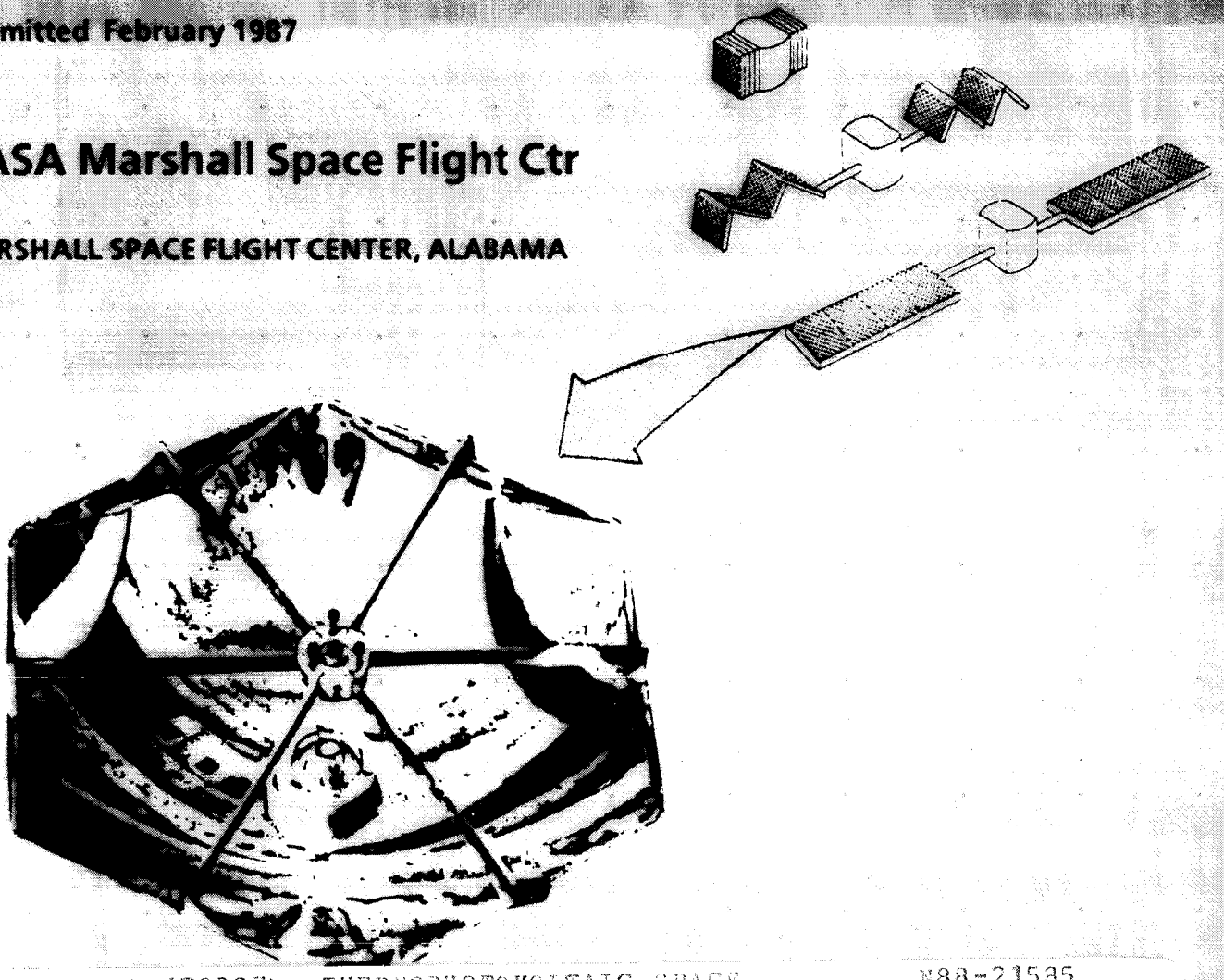

BOEING

Seattle, Washington

FINAL REPORT

NAS8-33436

THERMAL PHOTOVOLTAIC SPACE POWER SYSTEM

Prepared by

W. E. Horne
C. Lancaster

Submitted to

NASA Marshall Space Flight Center
Marshall Space Flight Center, Alabama

February 2, 1987

Boeing Aerospace Company
Seattle, Washington 98124

TABLE OF CONTENTS

LIST OF FIGURES

LIST OF FIGURES (Continued)

LIST OF FIGURES (Continued)

LIST OF FIGURES (Concluded)

1.0 INTRODUCTION

The solar thermophotovoltaic (STPV) space power concept operates on the principle of: (1) shifting the solar spectrum to better match the bandgap of a photovoltaic cell by means of an intermediate absorber/emitter which reradiates by incandescence and (2) recycling out-of-band energy by means of a reflective cavity. This concept offers theoretical efficiency in excess of 50%. Practical efficiencies on the order of 30% or greater are expected. These efficiency ranges, coupled with lightweight concentrator technology leads to power-to-weight ratios in excess of 300 W/kgm which exceeds intermediate goals of both NASA and the Air Force. It also offers power densities on the order of 400 W/m^2. The encapsulation of the photovoltaic cells inside the TPV cavity offers shielding against the natural particulate radiation environment to increase mission life.

At Boeing, a study has been underway for several years. This study has approached the STPV from a system or module point of view rather than strictly cell development. At present all the engineering questions regarding TPV operation have been answered. A 14% operating STPV has been demonstrated. It appears that only a custom designed cell (the Boeing work to date has used off-the-shelf cell technology) is required in order to realize the efficiencies promised by the STPV concept. Figure 1-1 illustrates this observation. From the curve in figure 1-1 it can be seen that the efficiency is a nonlinear function of the ratio of useful energy absorbed to parasitic losses in the cavity. The data in the figure show the progress made by optimizing cavity parameters during the Boeing program. At the present time the cavity appears to be near optimum so that further improvements in cell performance will give large improvements in STPV efficiency.

The module that was designed and tested is illustrated in figure 1-2. The module consists of a hexagonal parabolic primary reflector in a cassegrainian concentrator configuration. Heat

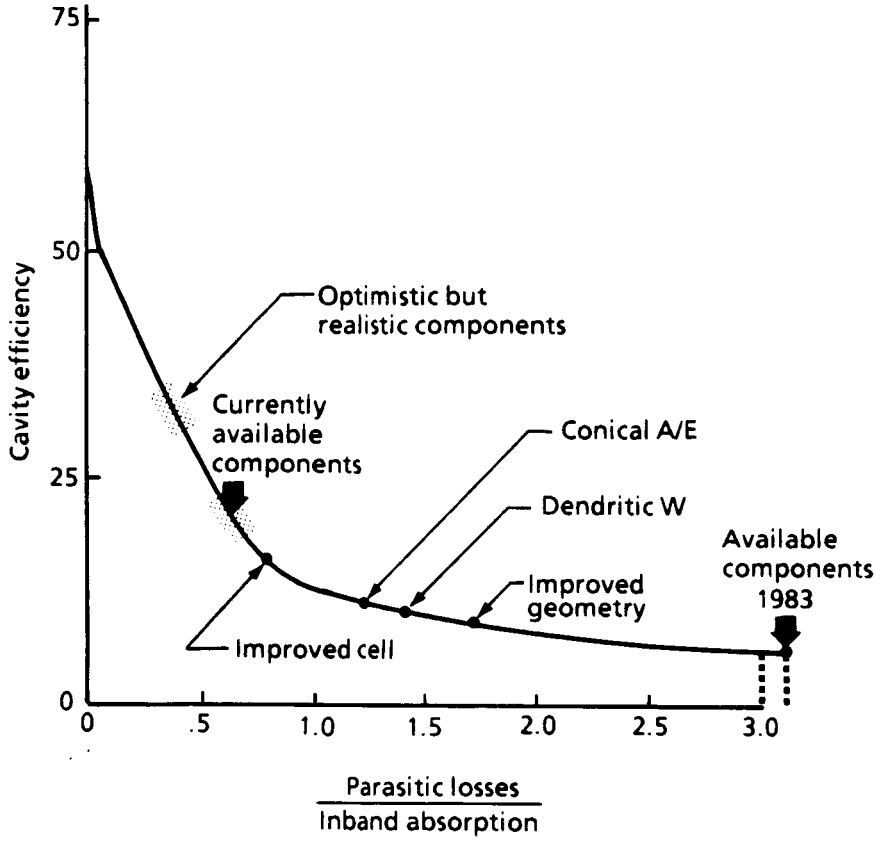

Figure 1-1. Boeing STPV Prototype Cavity Development Process

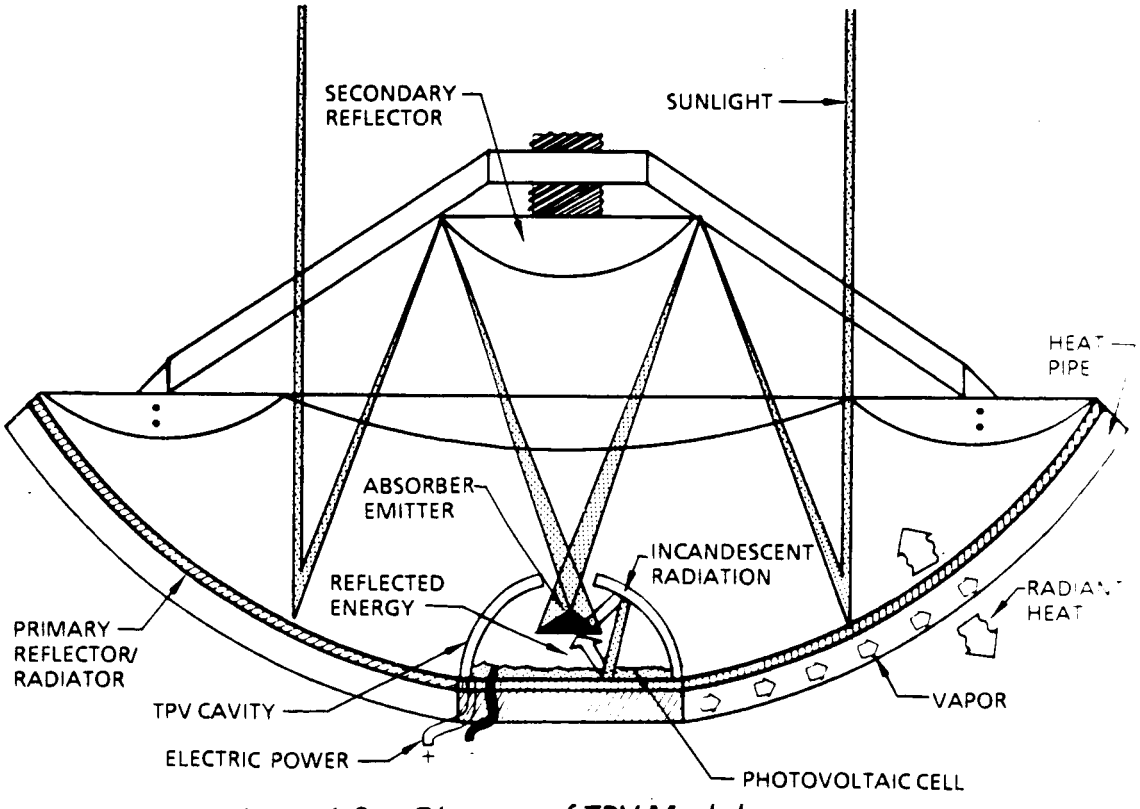

Figure 1-2. Diagram of TPV Module

pipes extending radially from the base of the TPV cavity base distribute heat to the primary collector which doubles as thermal radiator as well as solar concentrator. The concentrated sunlight is focused onto a dendritic tungsten absorber/emitter which heats to incandescence and radiates into a semielliptical cavity. A photovoltaic cell located at the base of the cavity converts short wavelength photons into electrical energy and reflects long wavelength photons back to the absorber emitter. Each element of the STPV module will be discussed in detail in the following sections of this report.

This report summarizes work performed on a research and development program to establish the feasibility of a solar thermophotovoltaic space power generation concept. The program has been multiphased. Earlier phases have been reported in an interim report.[1] For completeness, this report will summarize the earlier work and detail the work on the current phase as it pertains to and extends the earlier work. The contract effort has been complimented by a Boeing internally funded effort. Much of the experimental hardware and materials development was performed on the internal program. Experimental measurements and data evaluation were performed on the contracted effort. The objectives of the most recent phase of the contracted effort has been: (1) to examine the thermal control design in order to optimize it for lightweight and low cost; (2) to examine the concentrator optics in an attempt to relieve pointing accuracy requirements to ± 2 degrees about the optical axis; and (3) to use the results of the thermal and optical studies to synthesize a new STPV module design that is optimized for space application.

2.0 MODULE DEVELOPMENT

2.1 CONCEPT DESCRIPTION

The concept is called a solar-thermal-photovoltaic (STPV) converter. The system has two attractive features: First, the system has a blackbody converter which absorbs concentrated solar energy and reradiates it at a lower temperature than the original source (sun), thereby lowering the characteristic frequency of the emitted spectrum so that this energy can be more efficiently converted to electrical power by photovoltaic cells, the theoretical potential being in excess of 50%. Second, it is also resistant to the natural environment because the photovoltaic cells are completely shielded exposing only the solar collector and waste heat radiative surfaces to the environment.

The energy balance for the concept is shown schematically in figure 2-1. Basically the system consists of a cavity having a highly reflective inner surface. Over this reflective surface are placed silicon photovoltaic cells. The photovoltaic cells may be transparent to long wavelength photons or they may be filtered by a selective coating that is reflective to long wavelengths. At the center of the cavity is a blackbody converter. This converter absorbs the concentrated solar energy and heats up to an equilibrium temperature from 2000 K to 2300 K. It then radiates energy to the photovoltaic cells. The quantum efficiency of silicon cells is very high for converting the energy absorbed from the 2000 K to 2300 K blackbody spectrum into electrical energy. The energy content of the spectrum that is of lower energy (longer wavelength) than the bandgap of silicon is either transmitted through the cell to the reflective surface which reflects it back to the blackbody where it helps to maintain the equilibrium temperature of that blackbody or it is reflected by a selective filter coating on the cell. Thus, the "energy out" of the system is equal to the "electrical energy out" plus the heat produced in the photovoltaic cells and at the reflective surface. One of the keys to the efficient operation

is the recovery by the absorber of photons of wavelengths between 1.1 μm and 8 μm. This reduces the heating of the cells when exposed to the blackbody spectrum and, most importantly, allows this energy to be "recycled" by the blackbody absorber. The cell, in effect, acts as an optical knotch filter absorbing energy from the emitted blackbody spectrum only in that wavelength region where photovoltaic conversion is most efficient. The efficiency of the cell to that portion of the spectrum of wavelength shorter than 1.1 μm then becomes the upper limit of the TPV converter. Analysis shows that such efficiency can theoretically exceed 50%.

2.2 THEORY OF TPV CONVERSION

In theory, the conversion process in the TPV converter differs in two important ways from that of a conventional solar cell. Conventional solar-cell-array systems are limited by the inherently low quantum efficiency of semiconductors in the space solar spectrum. The quantum efficiency is low because not all of the energy of a photon above the electron-hole-pair-production threshold is used to produce electron-hole pairs. For example, a 0.3 μm photon only requires 25% of its energy for the actual electron hole pair production, as figure 2-2 indicates. The remaining energy (or power), which amounts to 75% for a 0.3 μm photon, appears as kinetic energy which ultimately must be removed as unwanted heat. As the wavelength becomes longer (energy approaches the bandgap energy), more of the energy per photon is used to produce the electron-hole pair. Since for photon energies below 0.3 μm only one electron-hole pair per photon is produced in silicon, the electron-hole-pair production process in silicon is inherently inefficient for the direct conversion of high energy spectra such as the solar spectrum. In fact, only 44% of the incident solar energy can be utilized in electron-hole-pair production in silicon.

This inherent inefficiency is illustrated in figure 2-3. The shaded area represents energy, or power, in the solar spectrum

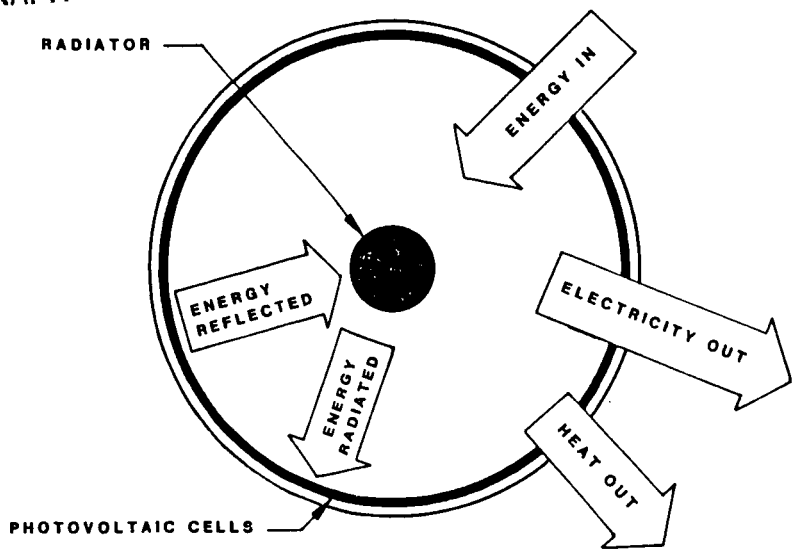

Figure 2-1. Energy Balance for TPV

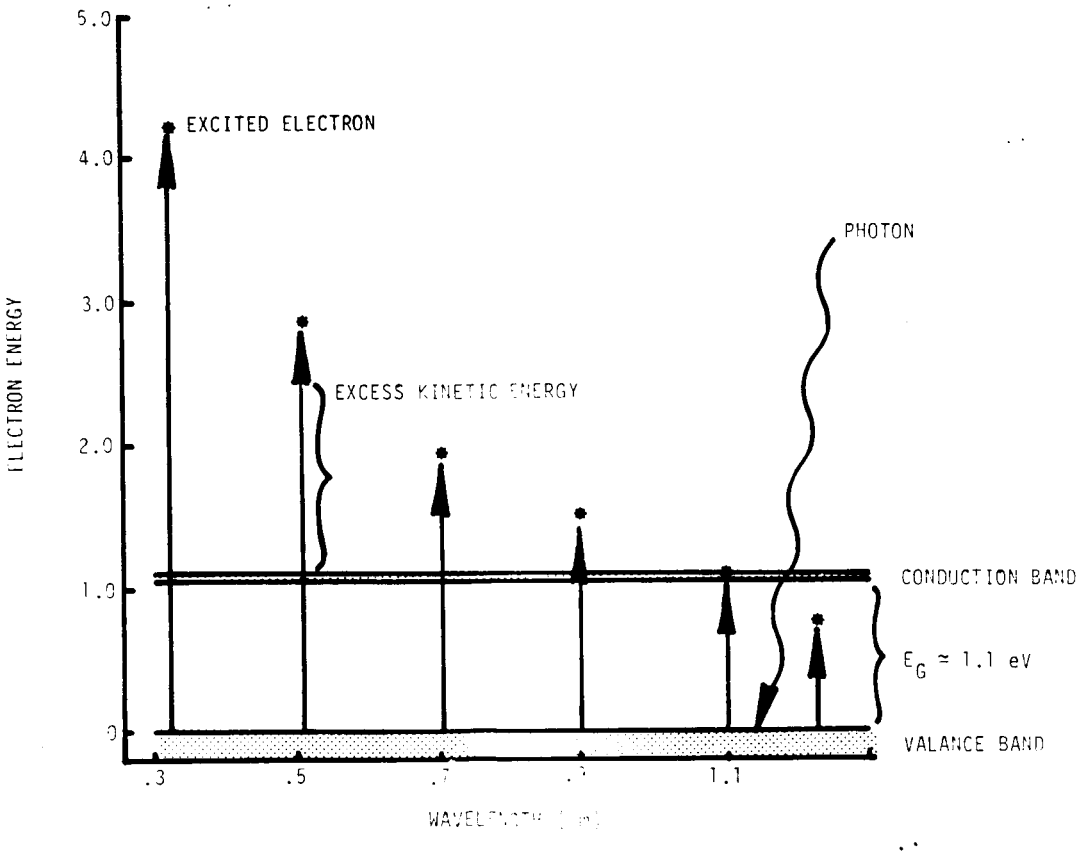

Figure 2-2. Photon Energy Use Profile Versus Wavelength in Silicon

(~ 6000 K blackbody) that is not available for conversion in a conventional silicon solar cell. The shaded area for wavelengths shorter than 1.1 μm represents that excess energy over the amount (1.1 eV) required by each photon to create an electron hole pair. The shaded area for wavelengths longer than 1 μm is lost because the photons no longer have sufficient energy to create electron-hole pairs. Thus, only the unshaded area (44%) is potentially available in the form of electron-hole pairs for photovoltaic conversion.

The maximum practical efficiency of the silicon cell to such a spectrum can be approximated by

$$N_{cell_{(max)}} \sim \frac{E_{HP}\ V_{OC} F}{E_{TS}(V_{BG})}$$

where E_{HP} = energy into hole pair production = 44% at 6000 K
E_{TS} = energy in total spectrum
V_{OC} = cell open circuit voltage (typically 0.6 V at 1 sun AMO)
V_{BG} = silicon bandgap potential ~ 1.1 eV
F = cell fill factor (typically 0.8)

$$N_{cell_{(max)}} \sim \frac{(0.44)(0.6)(0.8)}{(1.0)(1.1)} = 0.19$$

Considering the above discussion, two inherent properties of silicon can be exploited by the TPV concept to increase the overall efficiency of the photovoltaic-conversion process.

The first is that more efficient use of the photons of energy near the bandgap (1.1 μm) can be utilized by absorbing the solar energy to heat an incandescent absorber/emitter and by subsequent reradiation at a lower temperature thus shifting the radiation spectrum toward longer wavelengths as indicated in figure 2-4. As can be seen, for that portion of the spectrum of wavelength shorter than 1.1 μm, ~ 75% of the energy goes into electron-hole-

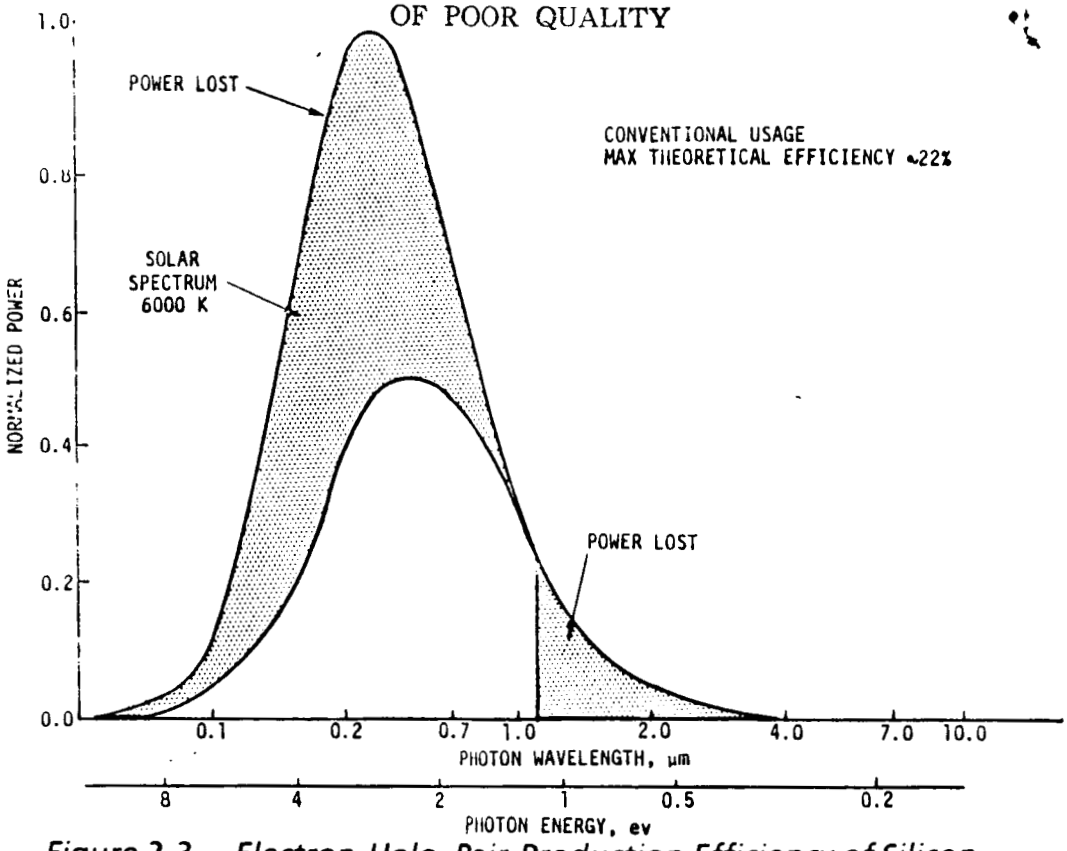

Figure 2-3. Electron-Hole- Pair-Production Efficiency of Silicon for AMO Spectrum

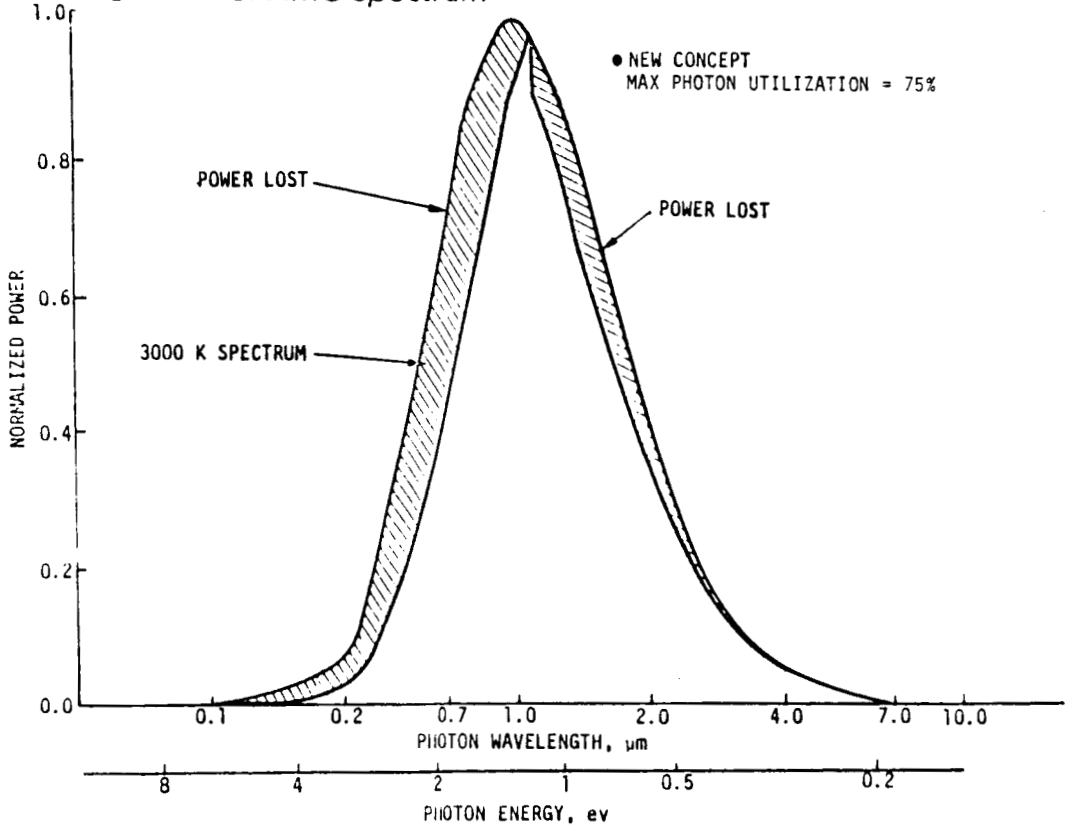

Figure 2-4. Electron-Hole-Pair-Production Efficiency of Silicon for 3000 K Blackbody Spectrum

pair production and this fraction will increase as the spectral peak shifts to longer wavelengths (lower temperatures).

The second is that, due to the transparency of reasonably pure silicon to photons of wavelength longer than 1.1 μm, the energy beyond 1.1 μm can be recovered by the TPV so that the overall practical efficiency of the solar cell discussed above can be greatly increased. The TPV concept recovers the long wavelength energy by reflecting it back to the incandescent radiator where it is reabsorbed. Thus, to the extent that the long wavelength energy can be reflected by the TPV cavity wall and transmitted through the silicon cells, the long wavelength energy is recovered. The TPV efficiency enhancement can be illustrated mathematically as follows:

$$N_{\substack{TPV \\ (max) \\ (3000\ K)}} \sim \frac{E_{HP}\, V_{OC} F}{E_{TS}\, V_{BG}\, (1 - E_{LW})}$$

where E_{LW} = fraction of the total spectral energy having
ϕ 1.1 μm (~ .5 for 3000 K)
= fraction of long wavelength energy recovered by absorber/emitter (0.95 appears reasonable)

NOTE: (E_{HP} 0.375 for 3000 K spectrum)

Thus, for the cell discussed above, a TPV with a 3000 K absorber/emitter would have a maximum efficiency given by

$$N_{\substack{TPV \\ (max) \\ (3000\ K)}} \sim \frac{(0.349)(0.6)(0.8)}{1 - (0.95)(0.5)} = 0.39$$

In actual TPV practice, the cell is operated in a concentrating mode so that $V_{OC} \geq 0.75$ V (at 500 suns) is more reasonable. Substituting this value in the above equation

$$N_{\substack{TPV \\ (max) \\ (3000\ K)}} \sim \frac{(0.349)(0.75)(0.8)}{1 - (0.95)(0.5)} = 0.49$$

Further, as the spectral energy is shifted toward longer wavelength (lower absorber/emitter temperatures) this value increases somewhat. A peak value of above $^{N}TPV_{(max)} = 0.51$ has been derived by more rigorous treatment by three independent analyses.[2,3,4] The optimum absorber/emitter temperature range appears to be 2000 K to 2300 K.

Of course, in actual practice there are loss mechanisms other than those associated with the photovoltaic process discussed above.

Several system-level studies of the TPV system have been made.[2-7] Although the baseline configurations adopted for the studies varied, the general conclusions were that when all loss mechanisms in the converter system are accounted for, a converter efficiency $\geq$ 40% appears very probable. Thus, if a concentrator efficiency of 80% is assumed, an overall efficiency of $\geq$ 32% for solar-to-electric conversion appears very probable. A detailed physical model developed during this effort and described in section 7.0 confirms these conclusions.

2.3 PRIOR EXPERIENCE

2.3.1 General Survey

Although the concept of a solar-heated-thermal-photovoltaic generator is new, the concept of a thermal-photovoltaic generator, STPV, heated by other means has received considerable attention in the past.

Most of the available data in the literature, prior to the present Boeing work, was reported since approximately 1966.[8-14] Work reported centers primarily around the development of PIN germanium cells and oxide radiator structures for use in a gas-fired-thermal-photovoltaic generator. The oxide radiators were studied to obtain desired spectral emittance characteristics in the desired wavelength band for which germanium cells would be most efficient. This was pursued over a considerable time period with modest success. Reasonable line emission characteristics were obtained; however, the problem of mechanical fracture under thermal cycling plagued the coatings and was the object of continuing research. The PIN germanium cells studied were planar devices having interdigitated P and N contacts on the backside of the cell with an intrinsic region on the front of the cell from which the carriers were collected. Such a cell design represented a considerable departure from standard cell design and the laboratory cells produced exhibited several unexpected phenomena. For example, an unexpectedly high spectral response to short wavelength (~ 0.4 μm) radiation was observed as well as an unexpected drop in open-circuit voltage (V_{OC}) as the load current was reduced. The drop in V_{OC} was attributed to recombination at the front surface and to the excess charge distribution in the intrinsic base over the interdigitated back P and N regions. Contact problems were also experienced at high current densities. Spectral reflectance curves on the cells also revealed a very low transparency to wavelengths beyond the bandgap. Thus, although the cells were considered promising, considerable developmental work was needed before a workable cell could be produced in quantity.

In spite of material and cell development problems, the analyses of these workers did support the viability of the TPV generator if the above cited problems could be overcome. A more recent investigation has been reported[8] in which a silicon PIN cell design was studied. The investigators reported developmental research on a silicon PIN cell design similar to the germanium design previously discussed except the P regions were located on the top of the cell underneath the contact grids, but not spanning the grids in order to enhance the transparency of the cells to long wavelength photons. The first laboratory cells produced had low efficiencies; however, they exhibited reasonably good I-V characteristics at high current densities. The same dip occurred in V_{OC} with decreasing load current as was observed for the germanium PIN cells discussed earlier. The cells also exhibited an anomalous parasitic absorption of approximately 10% of the long wavelength photons. This transparency loss was attributed to repeated reflections of energy from the closely spaced contact grids on the cell's front. To overcome this problem a solution was proposed to move the P regions and contact to the backside of the cell in an interdigitated manner similar to germanium design discussed earlier. The cell design further deviated from standard technology in that fused silica layers were located between the interdigitated P and N layers on the back of the cell to facilitate reflection of the long wavelength photons from the reflective back contact, which was electro-deposited on the cell. It was then projected that if the cells could be produced from ultrapure silicon with lifetimes on the order of several milliseconds, then efficient TPV cells would result. This cell design is still undergoing developmental work. It was also concluded that if the cells could be improved, then the TPV concept is viable and can produce solar-to-electrical conversion efficiencies on the order of 50%. To date these investigators have achieved 30% efficient cells operating in an ideal TPV cavity.

2.3.2 Boeing STPV Experience

2.3.2.1 General Module Description. At Boeing, a study has been underway for several years. This study has approached the TPV from a system or module point of view rather than strictly cell development. At present all the engineering questions regarding TPV operation have been answered. A 12.6% operating solar TPV (STPV) has been demonstrated. It appears that only a custom designed cell (the Boeing work to date has used off-the-shelf cell technology) is required in order to realize the efficiencies promised by the STPV concept. Figure 1-1 illustrates this observation. From the curve in figure 1-1 it can be seen that the efficiency is a nonlinear function of the ratio of useful energy absorbed to parasitic losses in the cavity. The data in the figure show the progress made by optimizing cavity parameters during the Boeing program. At the present time the cavity appears to be near optimum so that further improvements in cell performance will give large improvements in STPV efficiency.

The module that was designed and tested is illustrated schematically in figure 1-2. The module consists of a hexagonal parabolic primary reflector in a cassegrainian concentrator configuration. Heat pipes extending radially from the base of the TPV cavity base distribute heat to the primary collector which doubles as thermal radiator as well as solar concentrator. The concentrated sunlight is focused onto a dendritic tungsten absorber/emitter which heats to incandescence and radiates into a semielliptical cavity. A photovoltaic cell located at the base of the cavity converts short wavelength photons into electrical energy and reflects long wavelength photons back to the absorber emitter. Each element of the STPV module will be discussed in detail in the following sections.

3.0 STPV CAVITY DESIGN

The STPV cavity design is illustrated in the diagram of figure 3-1a. It consists of a semielliptical cavity with a flat base located at the midpoint between the two foci of the ellipse. The photocells are located on this flat base. The emitter/absorber is located at the focus of the ellipse. Thus, the cavity is optically imaging and radiated energy is either absorbed by the photocell or returned to the emitter/absorber with a maximum of two reflections as indicated by the traces in figure 3-1a. Concentrated sunlight enters the cavity through a window just behind the focal point. The optically imaging cavity is needed for two reasons. It allows the photocells to be mounted on a flat plane and it allows the surface area of the cavity walls to be much greater than the surface area of the emitter/absorber. The relative surface areas are designed to minimize contamination due to emitter/absorber evaporation. This will be discussed in more detail in section 4.0. Such cavities have been fabricated and tested. A photograph of an experimental cavity is shown in figure 3-1b. In actual operation with silvered walls in a silvered base (no photocells) the cavity design has been measured to return greater than 85% of the emitted energy back to the emitter absorber. Figure 3-2 shows the emitter/absorber temperature operating in the STPV prototype module for various base surface properties. This experimental data shows that the cavity design is adequate and offers considerable design margin for achieving the desired operating temperatures when a photovoltaic cell with 90% infrared reflectance is available as is proposed for the in-space experiment. It is felt that this cavity design is near optimum and it will be incorporated directly into the in-space experiment design. The cavity will be formed from aluminum with vapor deposited copper on the walls. The vapor deposited copper will be plated up to a thickness that can be polished and overcoated with vapor deposited silver for maximum spectral reflectance.

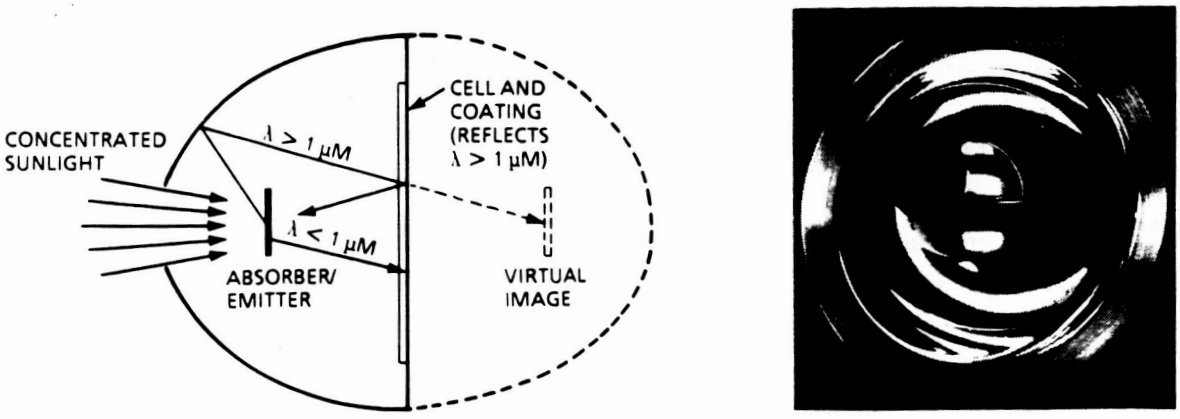

a) Diagram of TPV Cavity

b) Experimental TPV Cavity

Figure 3-1. TPV Cavity Configuration

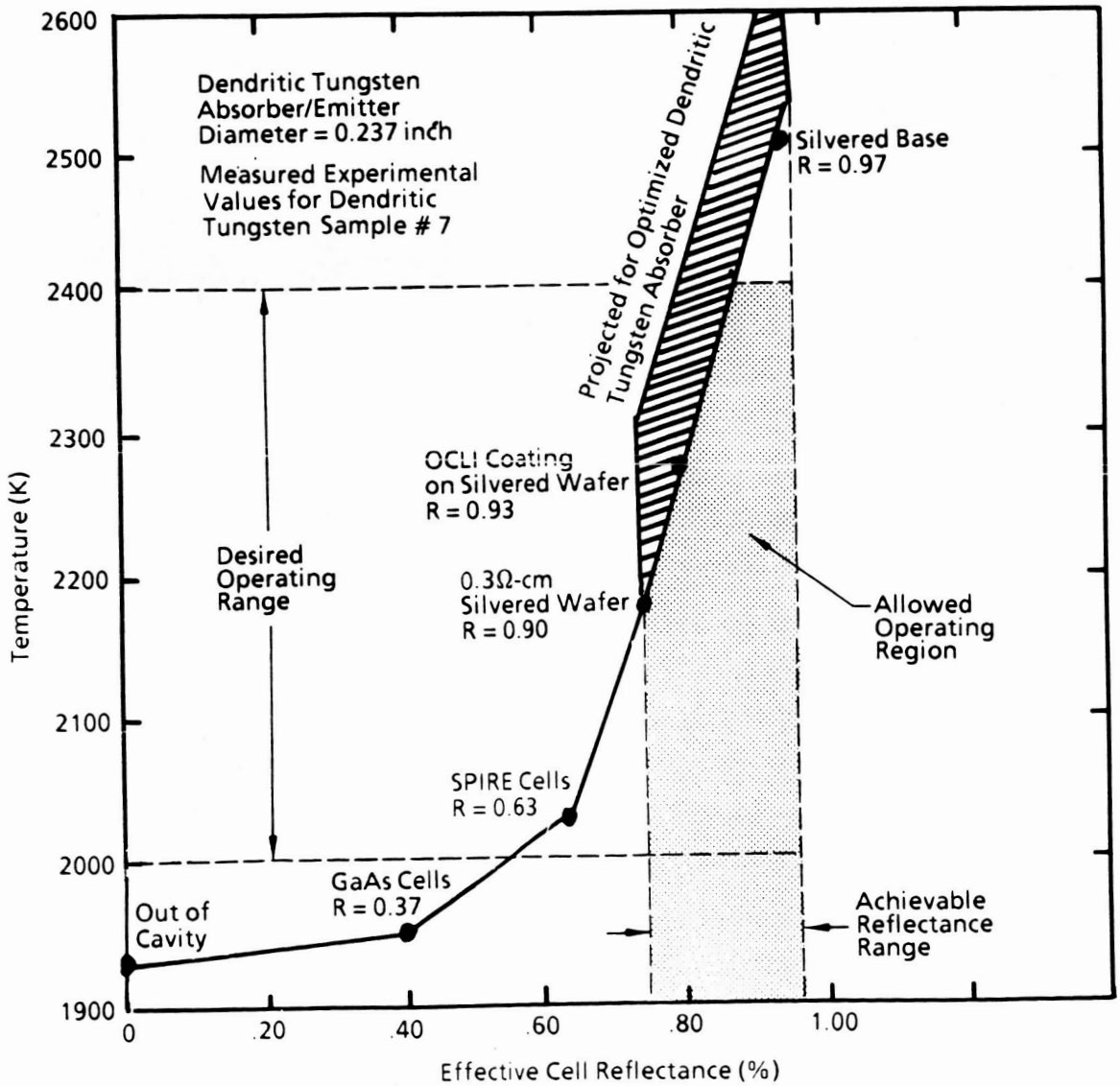

Figure 3-2. Cavity Performance Measurements for Dendritic Tungsten Absorber Emitter Diameter = 0.237 inch

4.0 EMITTER/ABSORBER DESIGN

The emitter/absorber is a critical component in the STPV design. It must operate for years over a temperature range from 2000 K to 2400 K and experience periodic cycles down to 0 K during orbital eclipse. It must also be mounted sturdy enough to withstand the stresses of launch yet be fragile enough to minimize thermal conduction losses through the mounting structure. The material best suited for these conditions is tungsten. The dendritic tungsten disk is mounted using 0.010 in diameter tungsten-rhenium wire as shown in figure 4-1a.

The absorber/emitter should also be highly absorbing over the solar spectrum (0.3 to 2.0 μm) and, ideally, it should suppress emission at long wavelengths (beyond 2.0 μm). In order to accomplish these functions dendritic tungsten crystals are grown on the surface of the tungsten absorber/emitter. Figure 4-1b shows a scanning electron microscope photograph of such a surface. The dendritic crystals are on the order of 100 microns tall and 10 microns spacing. Such a surface results in the absorptance curve shown in figure 4-1c. The solid curves show the absorptance of the dendritic tungsten curve compared to smooth, bare tungsten. As can be seen, the absorptance at short wavelengths is greatly enhanced while the long wavelength absorptances are comparable. Thus, the dendritic surface successfully absorbs solar energy and suppresses reradiation at long wavelengths yielding an emitted spectrum much richer in useful short wavelength photons as indicated by the dashed lines in figure 4-1b.

A major concern for the STPV cavity is contamination due to evaporation from the dendritic tungsten surface. For this reason, a life test is being conducted on a dendritic tungsten sample. The life test configuration is shown schematically in the drawing of figure 4-2 and one of the actual samples in the photograph. The tungsten samples are formed as a filament and heated electrically. Coverglasses are mounted at a fixed

a) Absorber/Emitter Mounting

b) Absorber/Emitter Dendritic Tungsten Surface

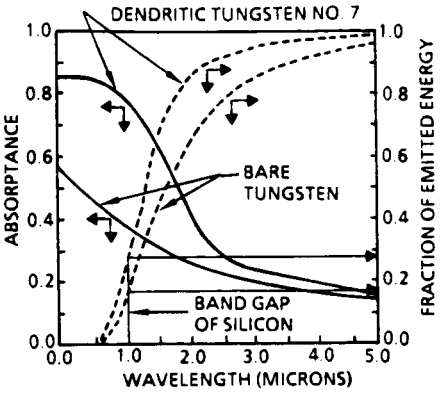

c) Absorptance of Dendritic vs Smooth Tungsten Surface

Figure 4-1. Absorber Emitter Characteristics

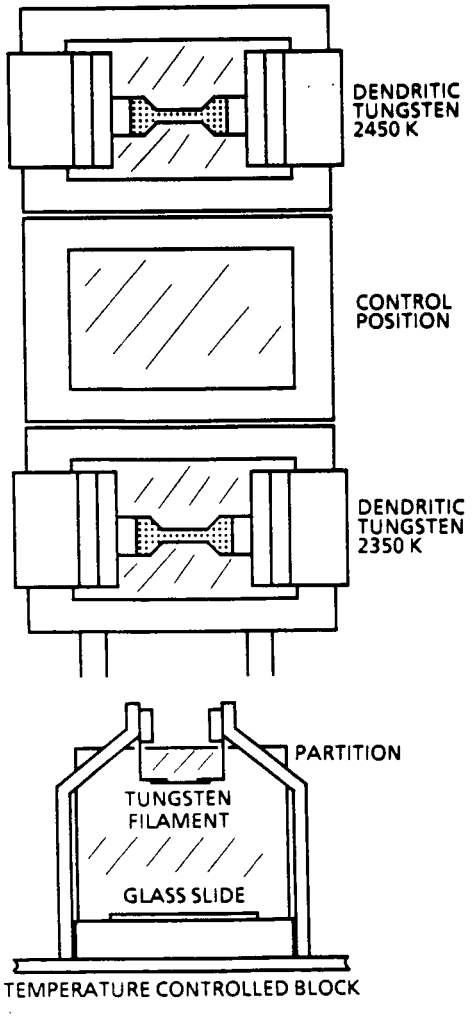

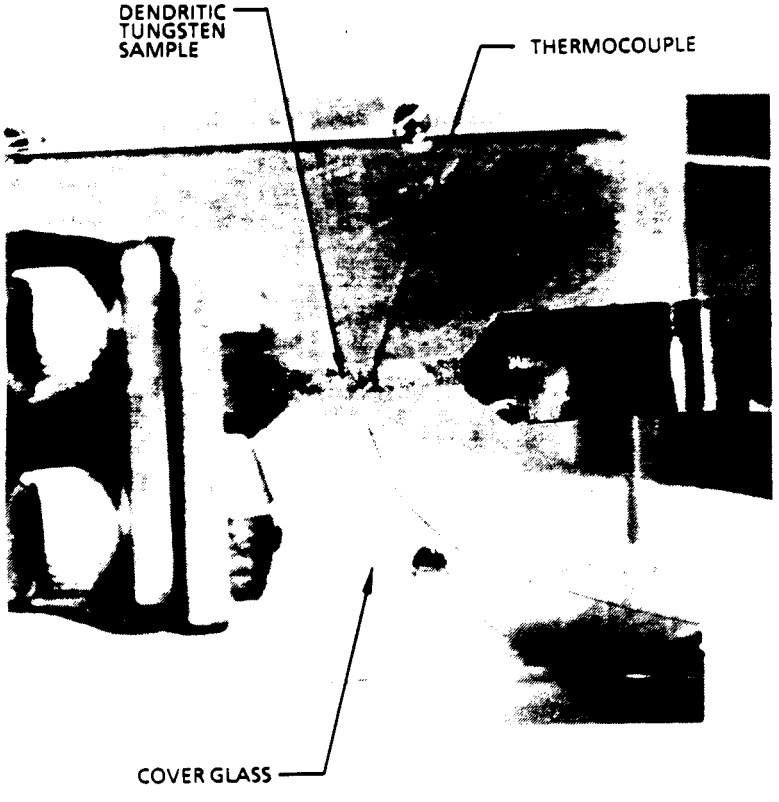

Figure 4-2. Absorber Emitter Life Test Configuration

distance below the samples. One-half of the surface of these coverglasses is coated with vapor deposited silver just as the cavity walls are. These glasses can be removed periodically and transmittance and reflectance measurements made to evaluate contamination. A third coverglass is mounted in a position that is shielded from the filaments by two partitions. This coverglass serves as a control and is measured along with the exposed glasses to evaluate contamination from sources other than the filament. The life test is conducted in a turbomolecular pumped vacuum chamber at ~ 10^{-7} vacuum. The test has been operating approximately one year and indicates that for a cavity wall surface area to emitter/absorber surface area ratio of 400 to 1 a lifetime in excess of 10 years can be expected. The optically imaging cavity described in the previous section is designed to permit this surface area ratio.

The proposed in-space experiment STPV absorber/emitter will be designed using dendritic tungsten. The three-dimensional analytical model described in section 7.0 will be used to synthesize a design that will take advantage of the directional emittance of the dendritic tungsten to reduce cavity window losses. For example, previous measurements have shown that the short wavelength (solar) absorptance is almost independent of angle of incidence while the long wavelength (1 to 2 micron and greater) emittance is strongly dependent on angle being greatest normal to the surface. Thus, by designing the absorber/emitter in a conical shape the incident solar energy admitted through the cavity window can be absorbed efficiently while the emitted long wavelength energy is directed away from the cavity window. Preliminary analyses indicate that the window losses can be reduced to as low as 2.7%. The conical dendritic tungsten absorber/emitter will be formed by chemical vapor deposition onto a mandrel. This technique has been developed by Ultramet Corporation.

5.0 PHOTOVOLTAIC CELL DESIGN

STPV operation requires a specially adapted photovoltaic cell design. The cell must have very good spectral response near its bandgap and it must be reflective to photons of energy less than its bandgap. Generally, due to their shorter absorption lengths, direct bandgap solar cells such as AlGaAs/GaAs cells have excellent response near their bandgap. Silicon on the other hand has weak absorption near its bandgap and hence is more difficult to make efficient near its bandgap. AlGaAs/GaAs cells unfortunately have to wide a bandgap and require too high a temperature on the absorber/emitter. A cell made from GaAsSb would have a bandgap of approximately 1.4 eV and would perhaps be ideal for STPV application; however, no cells are available in the near future from this material. In the interim, cells based on silicon have been used by Boeing for STPV prototype testing. The best cells that have been available to Boeing, fabricated by SPIRE Corporation, had only 73% specular reflectance in the infrared (reflectance greater than 90% are required for good STPV efficiency). Nevertheless, these cells were useful in engineering design evaluation testing of the prototype STPV module. Figure 5-1 shows a photograph of one of these cells mounted for testing.

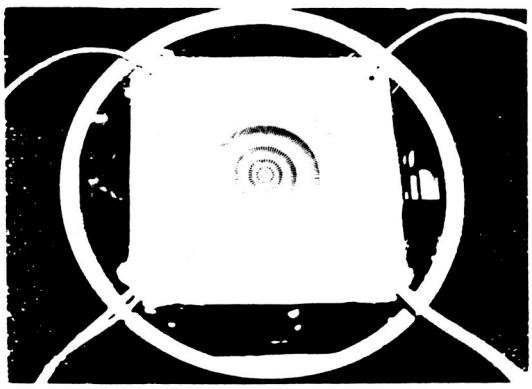

a) Photo of Experimental TPV Cell Mounted for Testing

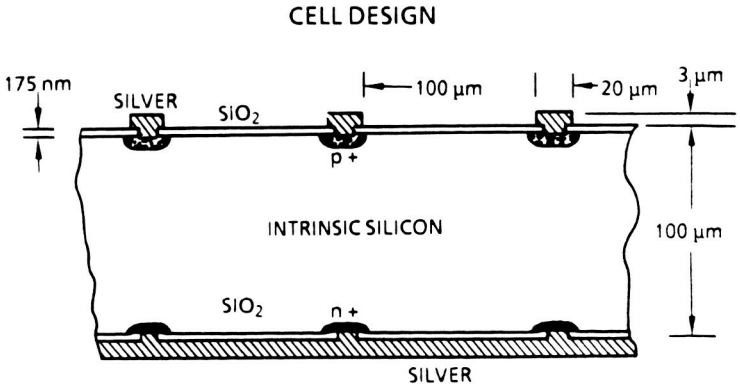

b) Diagram of Proposed TPV Photovoltaic Cell

Figure 5-1. TPV Photovoltaic Cell

Concurrent with the above module development and testing, workers at Stanford Research Center (as discussed in sec. 2.3.1) have developed a silicon TPV cell.[8] The basic design for these cells is illustrated in figure 5-1b. These cells achieved 96% infrared reflectance and demonstrated 30.5% efficiency operating in an ideal TPV cavity. The Stanford workers felt that the cell TPV efficiency could easily be increased to ~ 40%. However, due to a shift in funding, their work was directed into straight silicon concentrator cells for direct terrestrial solar concentrator applications. Using the TPV cell design as a starting point, they developed a similar cell with point contacts that demonstrated 27% efficiency at 500 sun intensity earth sunlight. It is felt that this cell design is near optimum for the STPV cavity and would probably achieve 40% or better TPV conversion efficiency. Therefore, it is recommended that these cells be tested in the STPV cavity.

6.0 STPV MODULE TESTS AND ANALYTICAL MODEL VALIDATION

Using the technology and components described in the previous sections a complete prototype STPV module was fabricated and tested. The module is shown in the photograph of figure 6-1. The prototype module was mounted in a thermal vacuum chamber and illuminated by a specially collimated solar simulator. This simulator was developed at Boeing. It has a filtered close matched AMO spectrum. It is collimated to ± 0.25 degrees and can illuminate a circular field up to 13 in in diameter at one AMO solar intensity. The prototype module was tested with a variety of off-the-shelf photovoltaic cells and spectral filters as indicated in figure 6-2. The best cells available to this program were SPIRE silicon cells which had 73% spectral reflectance in the infrared. Greater than 90% spectral reflectance is required in order to achieve high efficiency STPV operation. However, with the available cells, efficiencies up to 13.6% were measured for the STPV module. These experimental data serve to validate the mathematical model of the STPV system described in section 7.0 and to indicate that there are no fundamental problems with the STPV concept. The engineering questions have been answered and operational parameters determined.

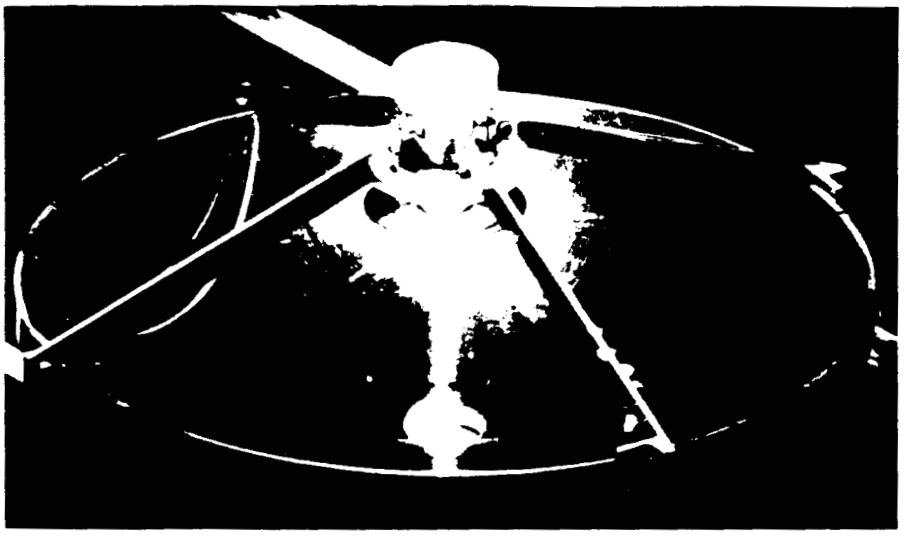

Figure 6-1. Photo of Experimental TPV Module Under Test in Boeing Collimated (± .25°) Solar Simulator Facility

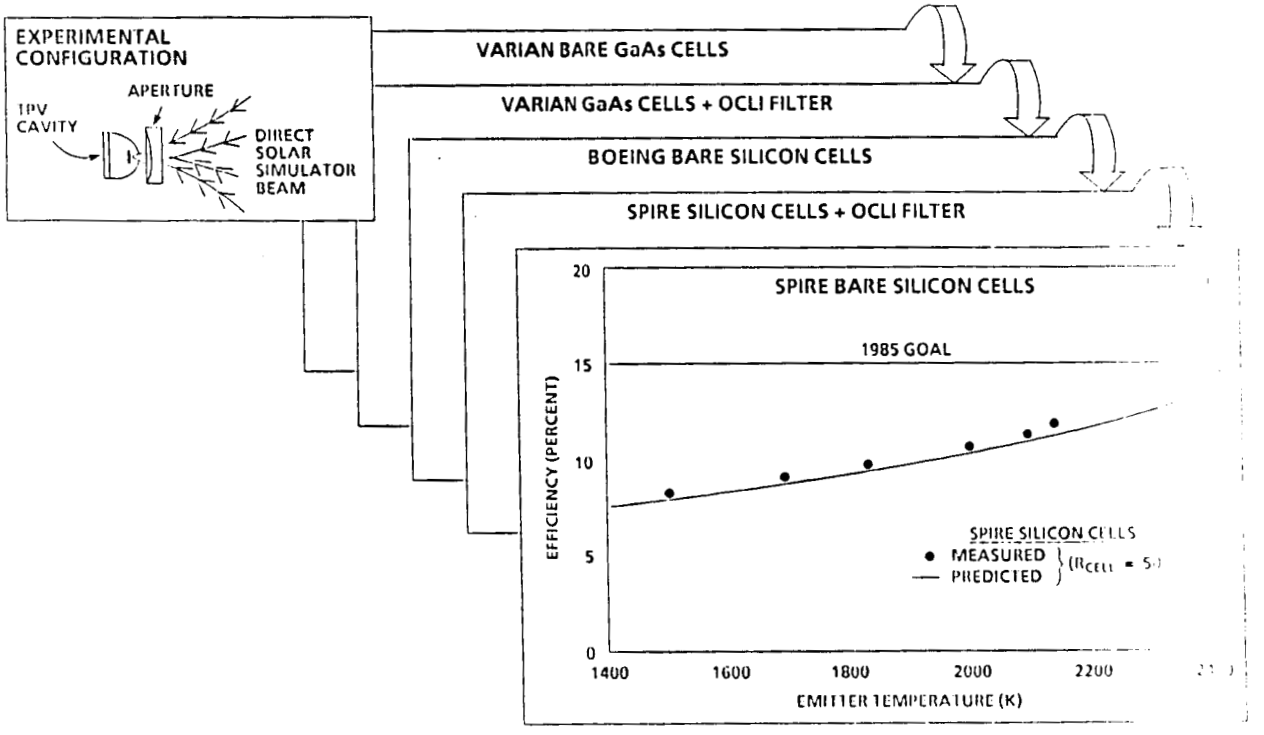

Figure 6-2. Experimental TPV Cavity Measurements

7.0 PHYSICAL MODEL OF STPV MODULE

In order to evaluate the STPV test results and predict performance with optimized photovoltaic cells, a mathematical model was developed.

The model of the STPV system accounted for the following items:

1. Variations in intensity of the sun's image.
2. Angular dispersion of the sun's image.
3. Specular absorption at the concentrator surfaces.
4. Diffuse reflectance of concentrator surfaces.
5. Manufacturing slope errors of concentrator surfaces.
6. Alignment errors in the concentrator system.
7. Solar absorptance of the absorber/emitter.
8. Emissivity of the absorber/emitter at operating temperature.
9. Reflection losses in the cavity reflective surfaces.
10. Radiation losses through the cavity aperture from cavity inner walls.
11. Radiation losses through the cavity aperture from absorber/emitter.
12. Reflection losses from cavity aperture.
13. Convection losses through absorber/emitter mounting structure.
14 Radiation losses from cavity aperture.
15. Spectral absorptance of photovoltaic cells.
16. Spectral response of photovoltaic cells.
17. Contamination of optical surfaces due to absorber/emitter evaporation.
18. Thermal heat rejection.
19. Thermal distortion of optical surfaces and alignment.

In addition to accounting for each of the above items, the model coupled each item of the system together since each unit is very closely coupled to the rest of the system. For example, the

quality of optics required in the concentrator is a function of how large the absorber/emitter can be made. The size of the absorber/emitter is a function of the desired operating temperature, the surface emissivity, and the amount of energy returned to it from the cavity walls.

Thus, the optical, thermal, and electrical properties of the concentrator and cavity must be coupled. The thermal control system is less sensitive to the above properties and, to a good approximation, can be treated separately from the primary optics and cavity parameters.

The model uses the solar image intensity profile shown in figure 7-1. This profile includes limb darkening and circumsolar. In the model, the profile is used as a probability density function along with a random number generator to select the angular dispersion of photons or rays to be treated in a ray tracing routine through the optical system. The energy of the rays is selected by a random number generator using the air mass zero (AMO) solar energy density spectral profile shown in figure 7-2. Thus, having selected the ray with respect to its angle of incidence and its energy, its absorption or reflection at each optical surface is treated by considering the spectral reflectance of each surface. Figures 7-3 and 4-1c show examples of the spectral properties used for the concentrator surfaces and for the absorber/emitter surface. Scattering of photons by surface slope errors and diffuseness is accounted for by introducing an rms slope error into each reflecting surface.

Once the solar energy is absorbed by the absorber/emitter, it must then be re-emitted by radiation from the absorber/emitter surface into the cavity. The emitted rays from the absorber/emitter surface must be characterized according to probability of emission, energy, angle, and location on the absorber/emitter surface. The probability of emission is handled by a random number generator coupled with a modified blackbody

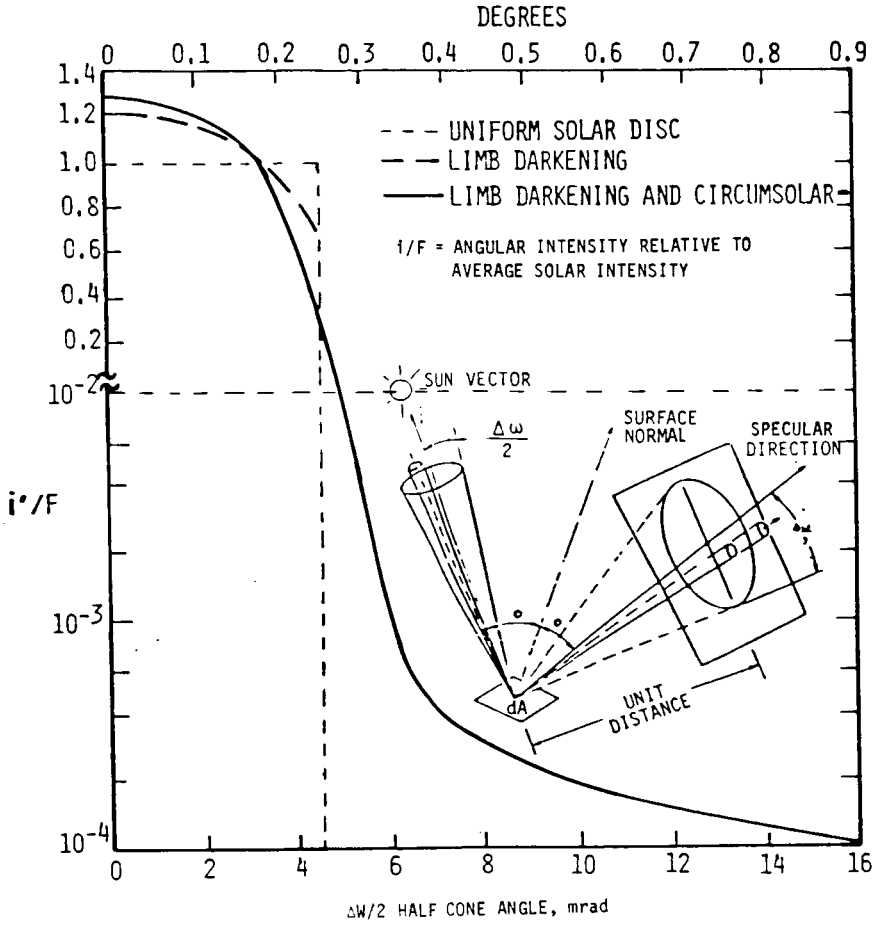

Figure 7-1. Solar Image Intensity Profile Used in Optical Analysis

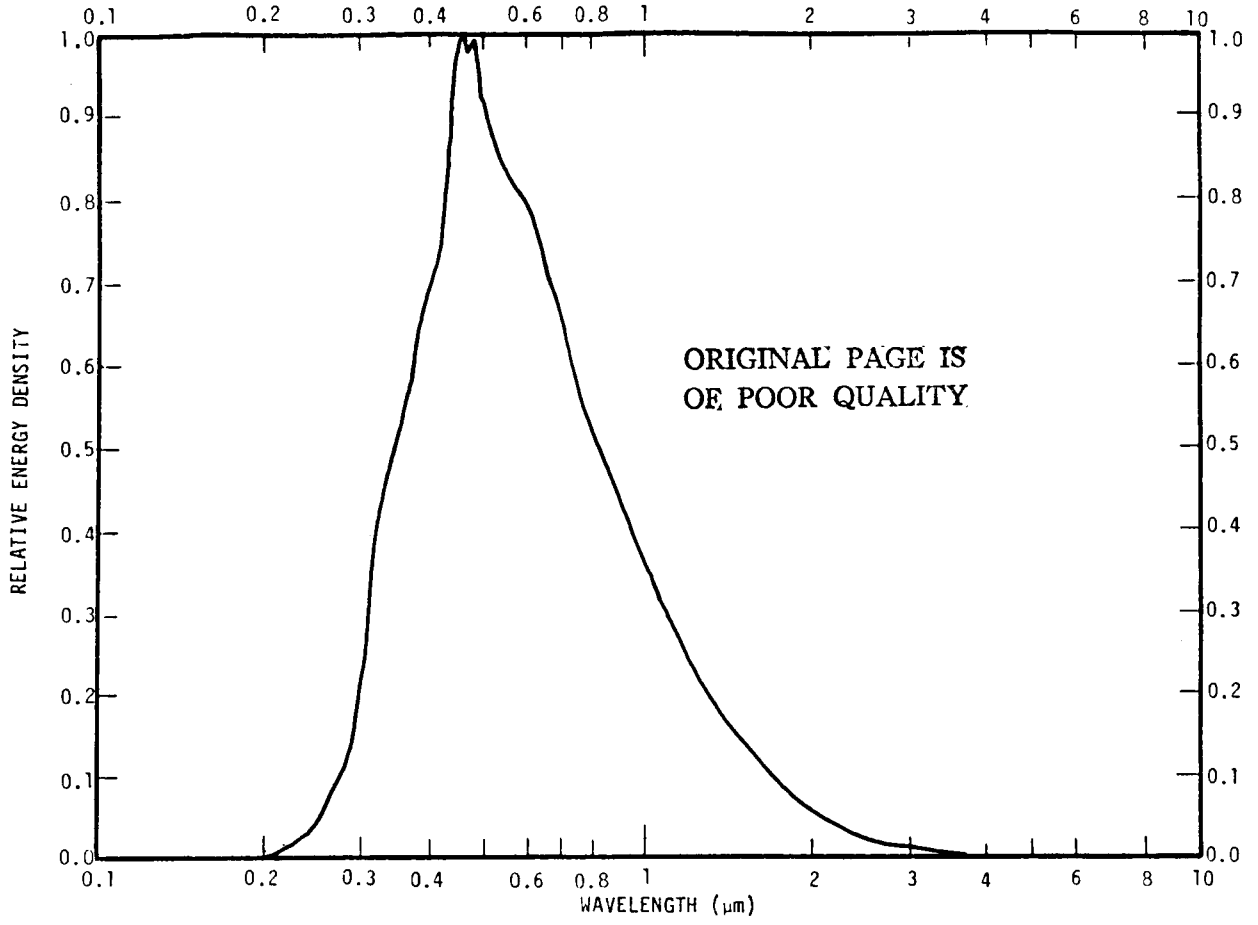

Figure 7-2. Air Mass Zero Solar Spectral Energy Distribution

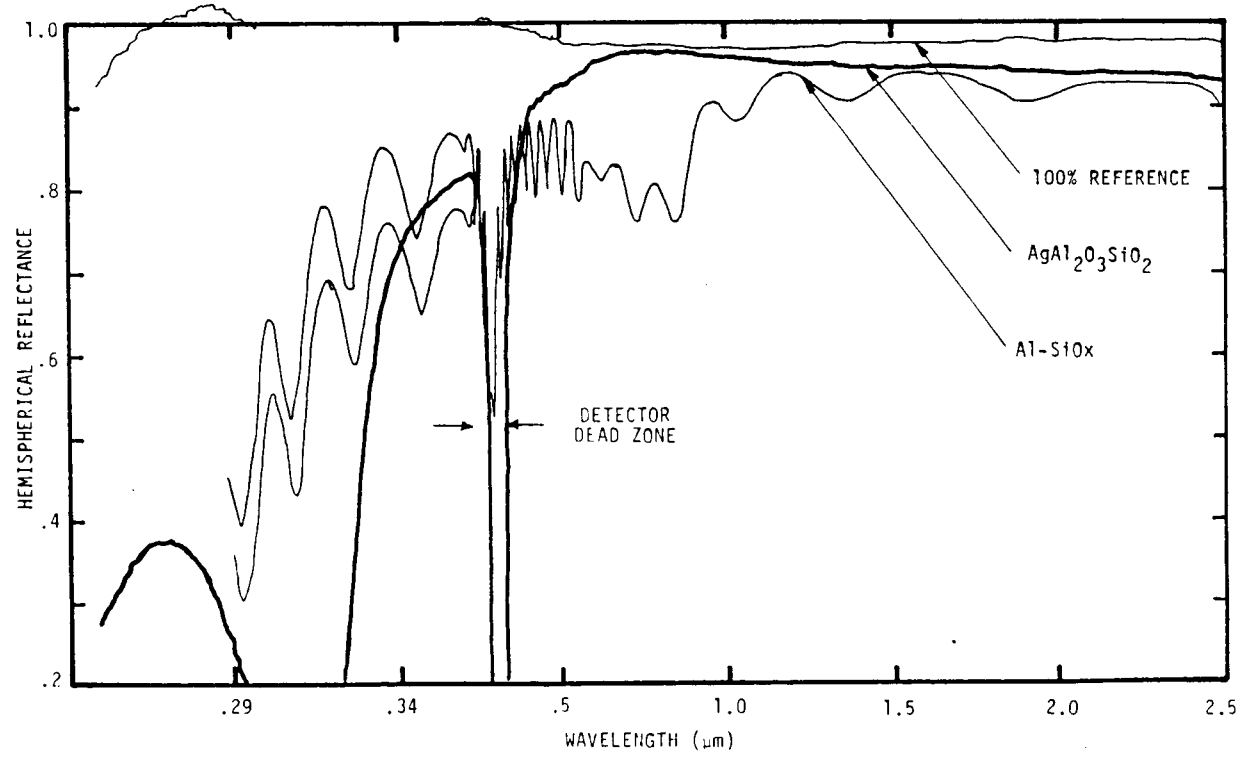

Figure 7-3. Comparison Of Reflectance for Al and Ag Coatings

energy density spectral profile. The modified blackbody energy density profile is obtained by multiplying the blackbody equation by the measured values of total hemispherical spectral emittance $\varepsilon(\lambda)$ for the material.

A normalized modified energy density profile for bare polished tungsten compared to that of a dendritic tungsten spectrum was shown in figure 4-1c. As an example for discussion, an absorber/emitter configured as a flat disc, illustrated in figure 7-4, is considered. The probability of a ray being emitted from a given face is determined by the ratio of the area of the face to the total surface area of the absorber/emitter. Once the face is selected, the x, y or z coordinates (as appropriate) are selected by a random number generator.

The angle of emission of the ray from the absorber/emitter surface is determined by a random number generator and the angular probability density distribution of photons emitted from the surface. As an example, for a typical Lambertian surface, the radiation intensity from an incremental surface area falls off as the cosine of the angle, θ, with respect to normal. At the same time, the solid angle $d\Delta$ contained in an annulus between θ and $\theta + d\theta$ increases as $\sin\theta$. Thus, if one considers the energy emitted through an incremental solid angle d as illustrated in figure 7-4, the angular energy distribution would have a $\sin\theta \cos\theta$ dependence on angle. Thus, a probability distribution of the form $\sin\theta \cos\theta$ is used with a random number generator to select the angle of emission with respect to the surface. Once this angle is selected, the direction of emission with respect to the other two axes is considered to be randomly uniform and is simply selected between 0 and 360 degrees by a random number generator. Thus, being defined in terms of wavelength and direction the emitted ray is then traced through the system as illustrated in figure 7-5. If it goes out through the window it is considered to be lost to the system. If it encounters the cavity wall the spectral reflectance of the wall is considered

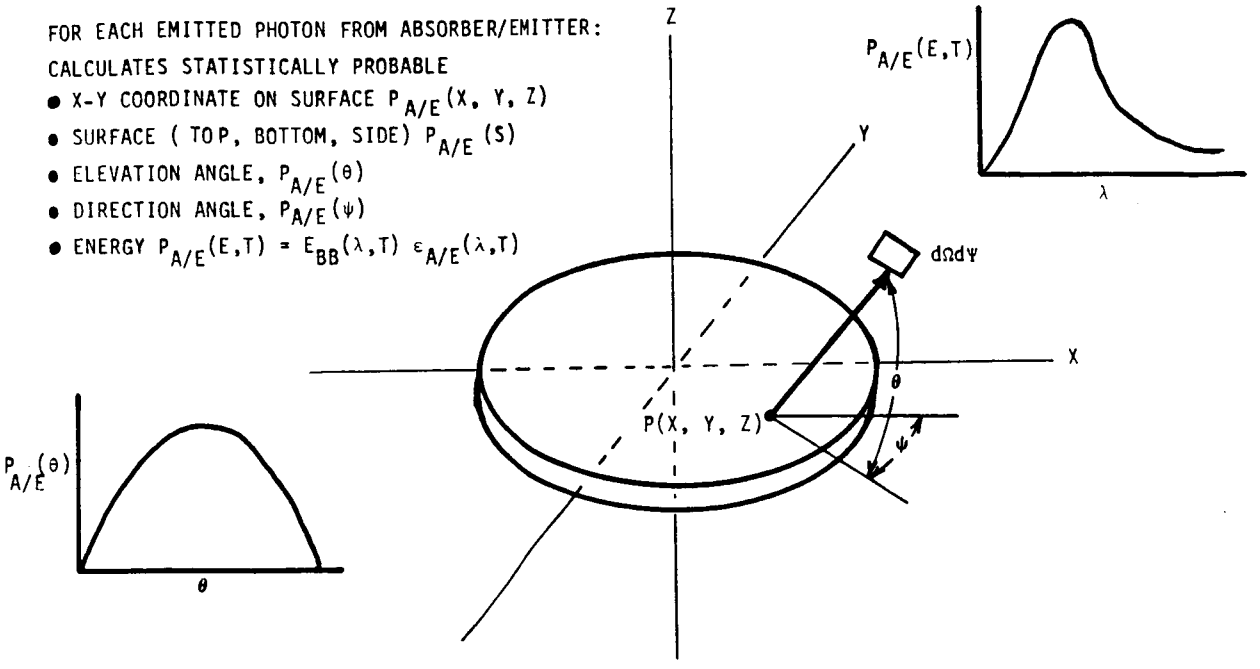

Figure 7-4. Three Dimensional Model of Absorber/Emitter

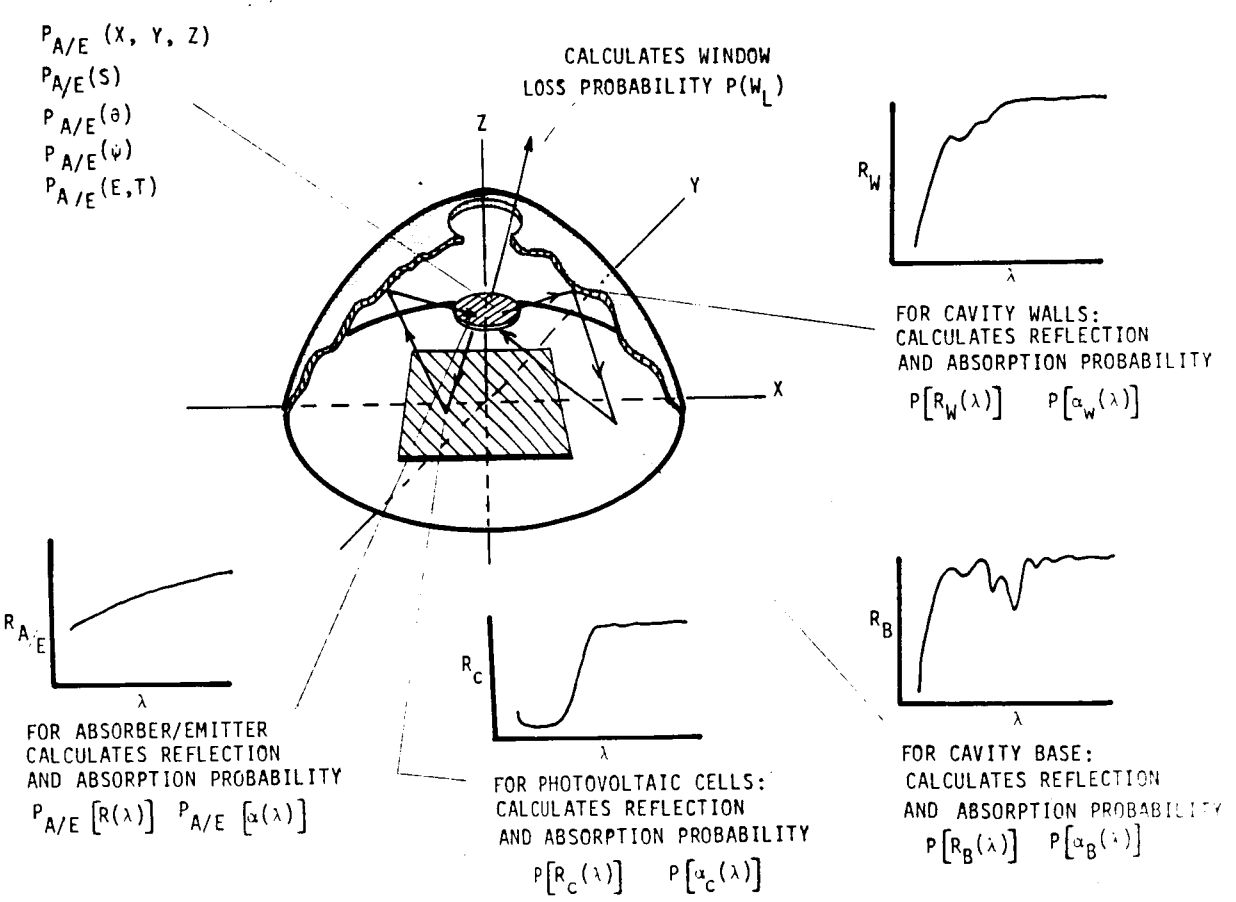

Figure 7-5. Three Dimensional Model of TPV Cavity

and the probability of absorption or reflection computed. If it is absorbed it is taken out of the system. If it is reflected it is traced to the next surface and the absorption/reflection computation repeated.

If the ray is absorbed in the photovoltaic cell then its energy is examined and if it is higher than the bandgap of the semiconductor then an electrical energy conversion is considered to be possible and the absorbed rays stored in bins according to their energy. Thus, the result of the cavity optical model is an inventory of the energy lost out the cavity window, absorbed as heat in each surface, absorbed in the useful band of the photovoltaic cell, or as returned to the absorber/emitter.

While the inventory of energy absorbed in various places is useful for design purposes, the desired result of the cavity optical/thermal model is an inventory by energy, or wavelength, of the photons absorbed in the photovoltaic cell. This inventory is integrated over the spectral response curve for the photovoltaic cell. Figure 7-6 shows a typical spectral response curve used for silicon cells. Thus, the electrical efficiency of the cavity is computed by

$$\text{Cavity Eff} = \left[\frac{\int_0^{\lambda_{BG}} E(\lambda)\, S(\lambda)\, d}{E_{in}} \right] \times V_{OC} \times FF$$

where $E(\lambda)$ = the energy spectrum of photons absorbed
$S(\lambda)$ = the spectral response of the cell
E_{in} = the energy into the cavity
λ_{BG} = the wavelength corresponding to the bandgap of the semiconductor
FF = the cell fill factor

For the overall system each of the above elements discussed above from the incident sunlight to the electrical energy out must be coupled together in order to study the overall effects of parametric variations on system performance (an exception being the thermal control model). Since the relative amount of thermal energy to be dissipated varies only a relatively small percentage with fairly large changes in TPV parameters, and the electrical response is modified relatively little by slight variations in temperature ($\Delta V_{OC}/ T \sim 2.5 \times 10^{-3} \Delta V/°C$ for Si) then the thermal control system can be adequately treated separately. Thus, the thermal analysis of the system is treated in a separate thermal control model.

Using this complete model for the system the module test conditions were used as input parameters and excellent agreement was reached between the model and the experimental measurements. Figure 6-2 illustrated this agreement.

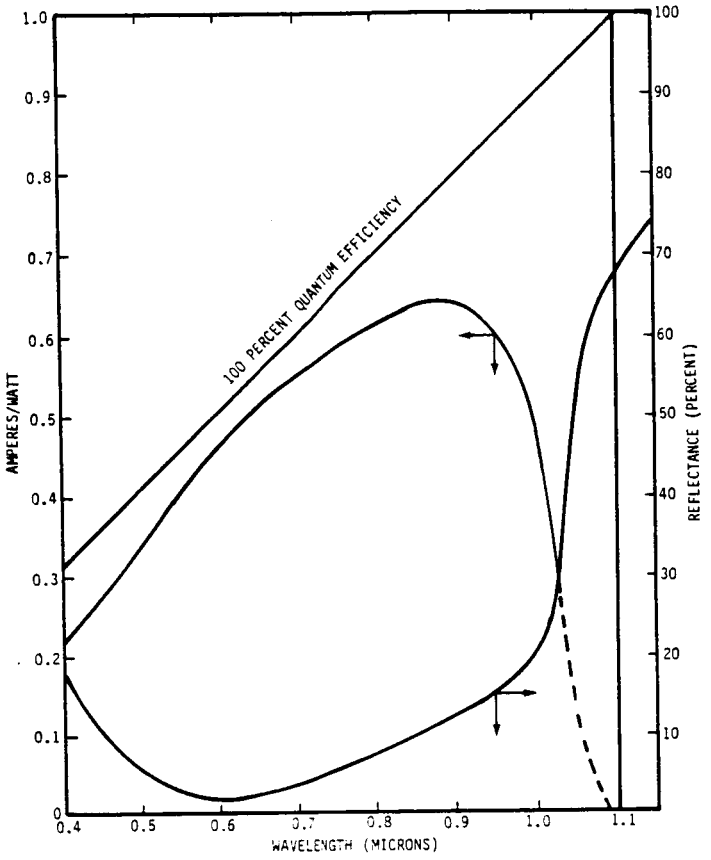

Figure 7-6. Measured Spectral Reflectance and Spectral Response for BSF Solar Cell

8.0 PREDICTED RESULTS FOR OPTIMIZED STPV

Having validated the physical model of the STPV module, the results that can be expected for an optimized cell in the STPV module were calculated. Figure 8-1 shows the conditions and results of one of these calculations. Thus, it is felt that efficiencies on the order of 34% can be realized with existing known technology.

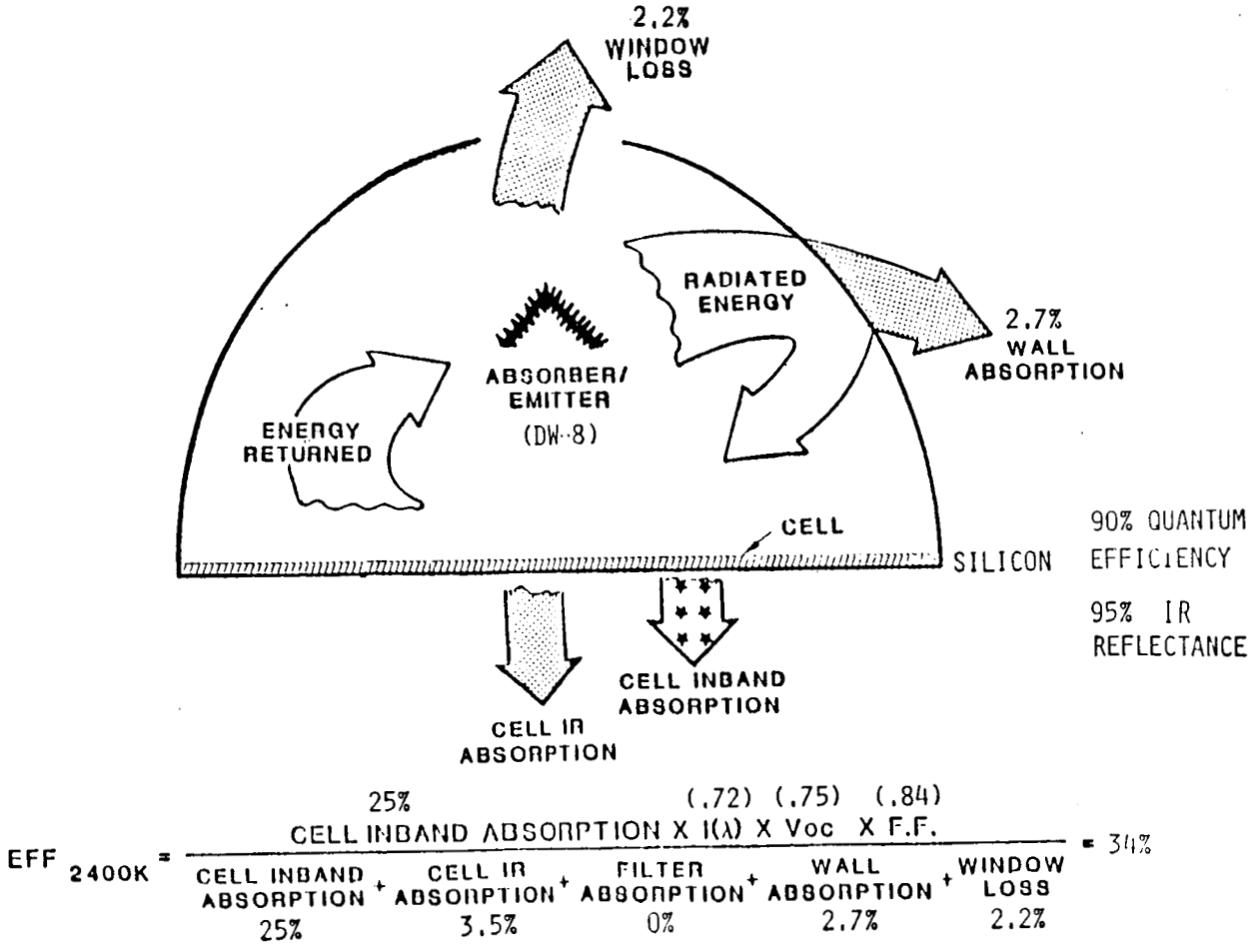

Figure 8-1. Summary of Input Parameters and Predicted Results for STPV In-Space Experimental Module

9.0 CONCENTRATOR OPTICS

The concentrator optics developed for the STPV are shown in figure 9-1. Figure 1-1 showed a schematic illustration of the concentrator. They consist of a cassegrainian system with a hexagonal primary reflector to facilitate close packing in an array. The substrates of these reflectors are fabricated by blow forming magnesium sheet over a performed die. These substrates are coated with vapor deposited silver and overcoated with SiO_x so that they not only reflect over the solar spectrum but they also act as a thermal radiator, or emitter with front surface emittance ~ 0.45 at 323 K where the system normally operates in-space. These units have been tested with SiO_x overcoated aluminum reflectors and found to have optical efficiencies of 76%. It is believed that efficiencies on the order of 85% can be achieved with Al_2O_3 overcoated silver reflectors. Details of the development of these concentrators have been reported in an interim report.

Figure 9-2 shows a schematic diagram of the system used to test the optical concentrator system. Both the primary and secondary lenses of the concentrator were overcoated with vapor deposited aluminum and SiO_x. From knife edge image displacement type measurements it was estimated that the maximum surface errors on the primary mirror surface were on the order of 4 mrad to 5 mrad. The computer analysis of the system, shown in figure 9-3, indicated that with zero pointing error, the system with ~ 7 mrad surface error could concentrate 80% (neglecting surface absorption) of the incident AMO sunlight into a 0.25 in diameter circle. Assuming that both the primary and secondary lenses have ~ 4 mrad of surface error as measured earlier for the primary then the system error would be $\sqrt{4^2 + 4^2}$ mrad or ~ 5.6 mrad. Figure 9-4 shows the relative amount of energy into apertures of varying diameter. As can be seen, at an aperture diameter of 0.25, about 88% of the incident rays (neglecting surface absorptance) are concentrated into the aperture. This percentage

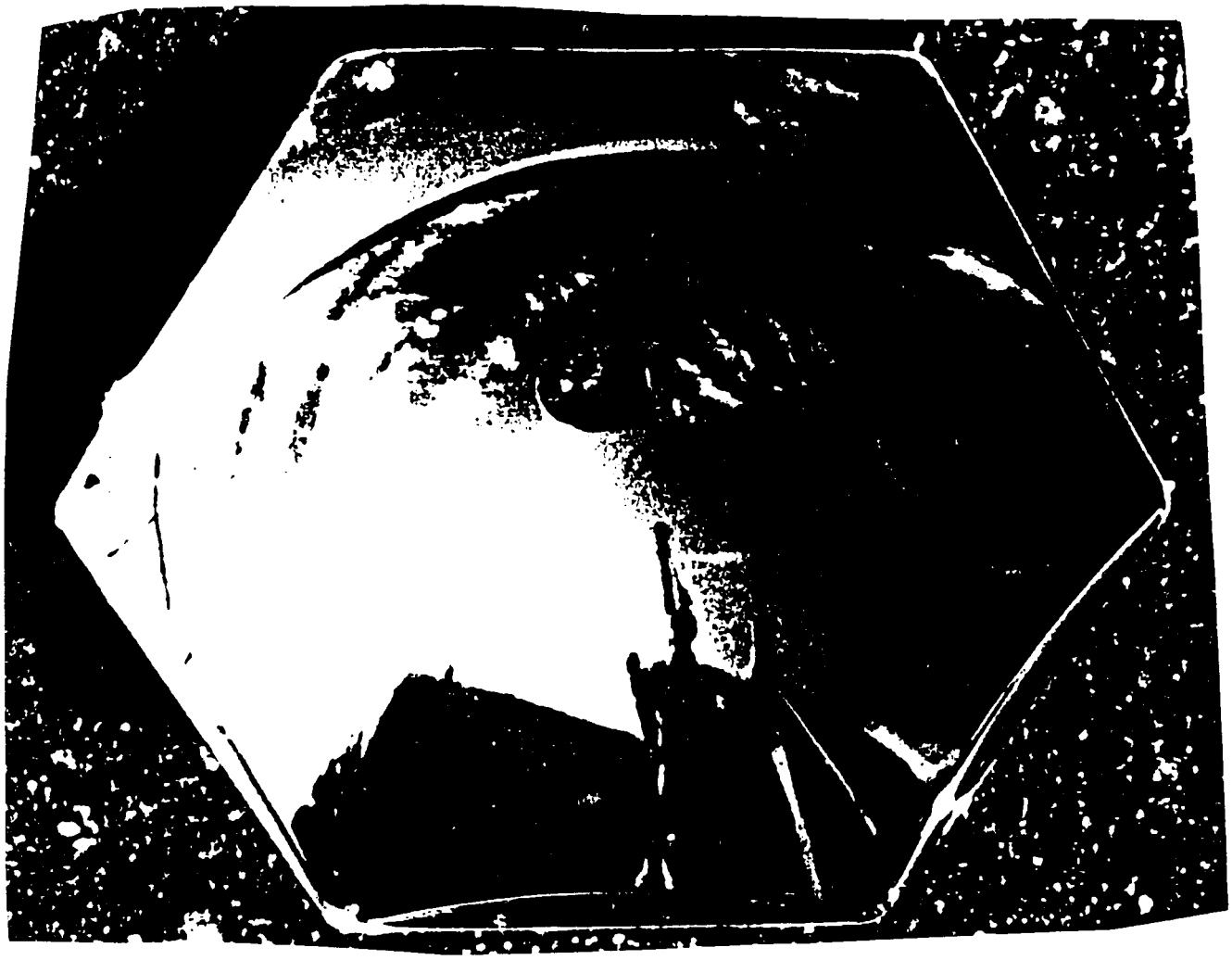

Figure 9-1. Overall View of Completed Reflector With Radiation Hard coatings (RMS Surface Error ∠ 1 mrad)

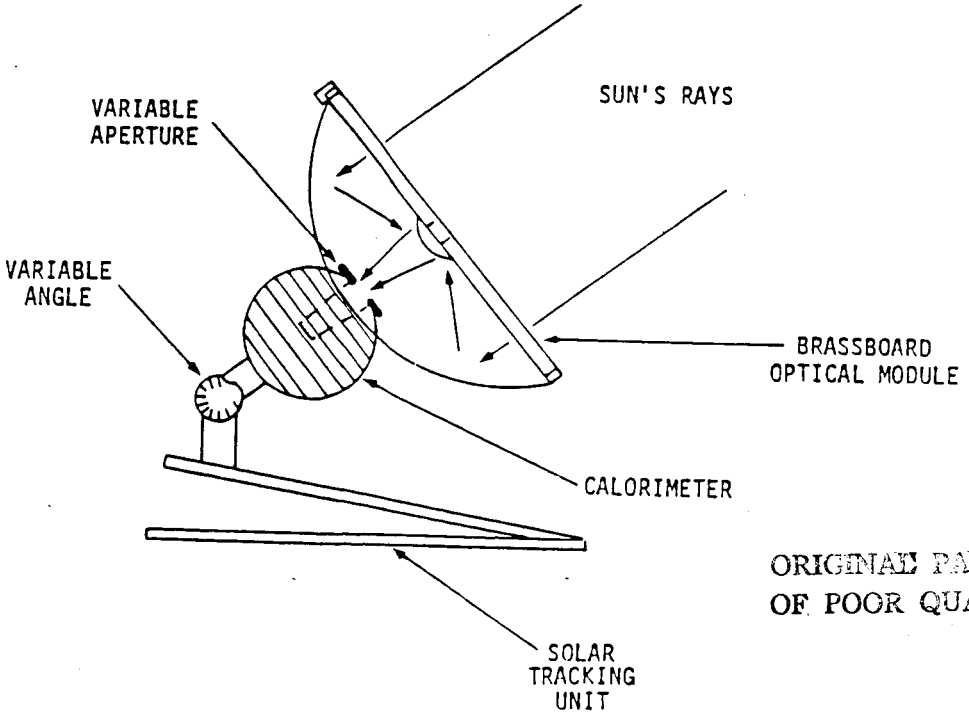

Figure 9-2. Diagram of TPV Brassboard Module Optical Evaluation Experiment

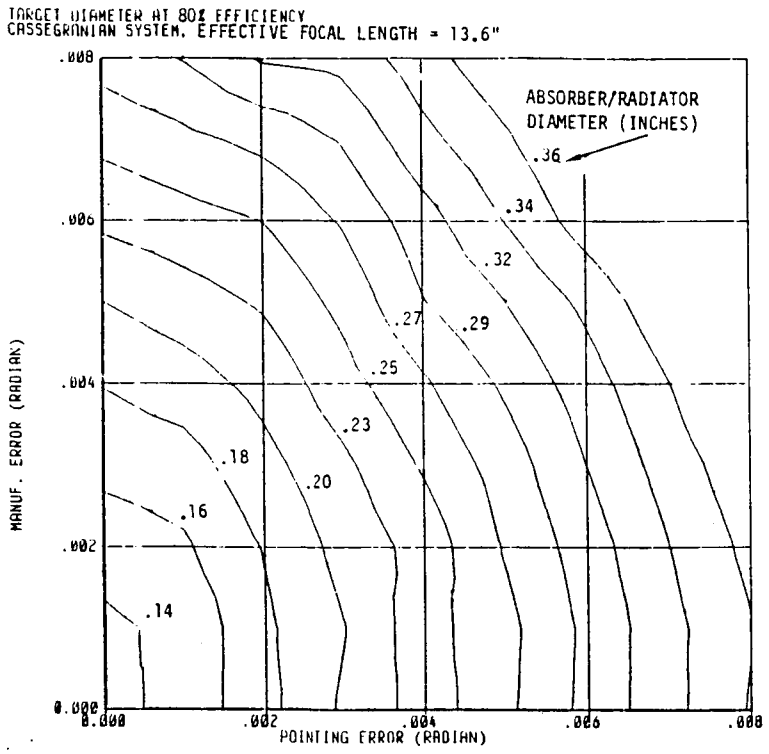

Figure 9-3. Error Tolerance of Optical Design for an Efficiency of 80 Percent (Energy Onto Target or Focal Point)

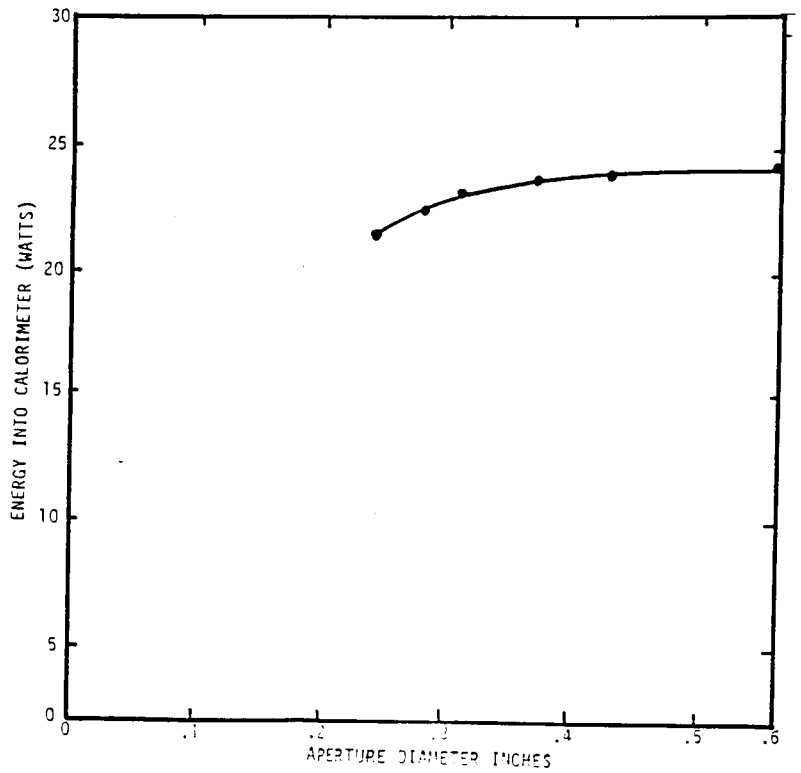

Figure 9-4. Energy Collection Efficiency for Concentrator System

indicates that the system has considerably less than the 7 mrad predicted for 80% efficiency by the parametric curves of figure 9-3. The overall system surface error of approximately 5.6 mrad from the knife edge image measurements appear to agree reasonably well with the concentrator performance measurements. These measurements were made on units from the early phases of the program when a female die was in use for substrate formation and hand polishing was required on the primary concentrator surface. Newer units are formed with a male die which requires no hand work and should have substantially less surface error; however, tests on these units have not been conducted.

Tests were also performed to determine the absolute concentrating efficiency of the system. Basically the energy incident on the system from August sunlight in Seattle was measured. Table 9-1 summarizes the results of these measurements. These measurements indicate an average surface reflectance of ~ .87 for each concentrator surface. This value is in good agreement with an integration over specular reflectance curves for the surfaces such as those shown in figure 9-5.

The concentrator efficiency values will be somewhat higher for AMO sunlight. The measured values indicated in table 9-1 are not corrected for the scattered component of sunlight due to passage through the atmosphere. The way that the incident sunlight intensity was measured in these experiments (using a single aperture in front of the calorimeter) did not permit a true separate measurement of direct unscattered sunlight. Proof that scattering did affect the measurements was found in a comparison of measurements made after a long dry period and measurements following a rainy period when the atmosphere was cleaner. The measurements shown in table 9-1 were made during a long dry period. A repeat measurement with a .563 in aperture after a rain indicated an efficiency of slightly greater than 76%, or about 2% higher than before the rain. Thus, it is felt that the overall efficiency numbers are probably about 5% higher than

Table 9-1. Solar Concentrator Evaluation Measurement

APERTURE SIZE (DIAMETER) (inches)	(cm)	MEASURED SUNLIGHT INTO CALORIMETER (watts)	CALCULATED TOTAL ENERGY INCIDENT (watts)	MEASURED CONCENTRATED ENERGY INTO CALORIMETER (watts)	MEASURED CONCENTRATOR COLLECTION EFFICIENCY (NEGLECTING SURFACE ABSORPTION)	MEASURED OVERALL CONCENTRATOR EFFICIENCY	OVERALL CONCENTRATOR EFFICIENCY CORRECTED FOR ATMOSPHERIC SCATTERING
.563	1.43	0.125	32.685				
.563	1.43	0.125	32.685	24.4	1.000	0.747	.786
.437	1.11	0.125	32.685	24.0	0.984	0.734	.773
.375	0.95	0.125	32.685	23.9	0.980	0.731	.769
.312	0.79	0.125	32.685	23.2	0.951	0.710	.747
.281	0.71	0.125	32.685	22.6	0.926	0.691	.727
.250	0.64	0.125	32.685	21.6	0.885	0.661	.696

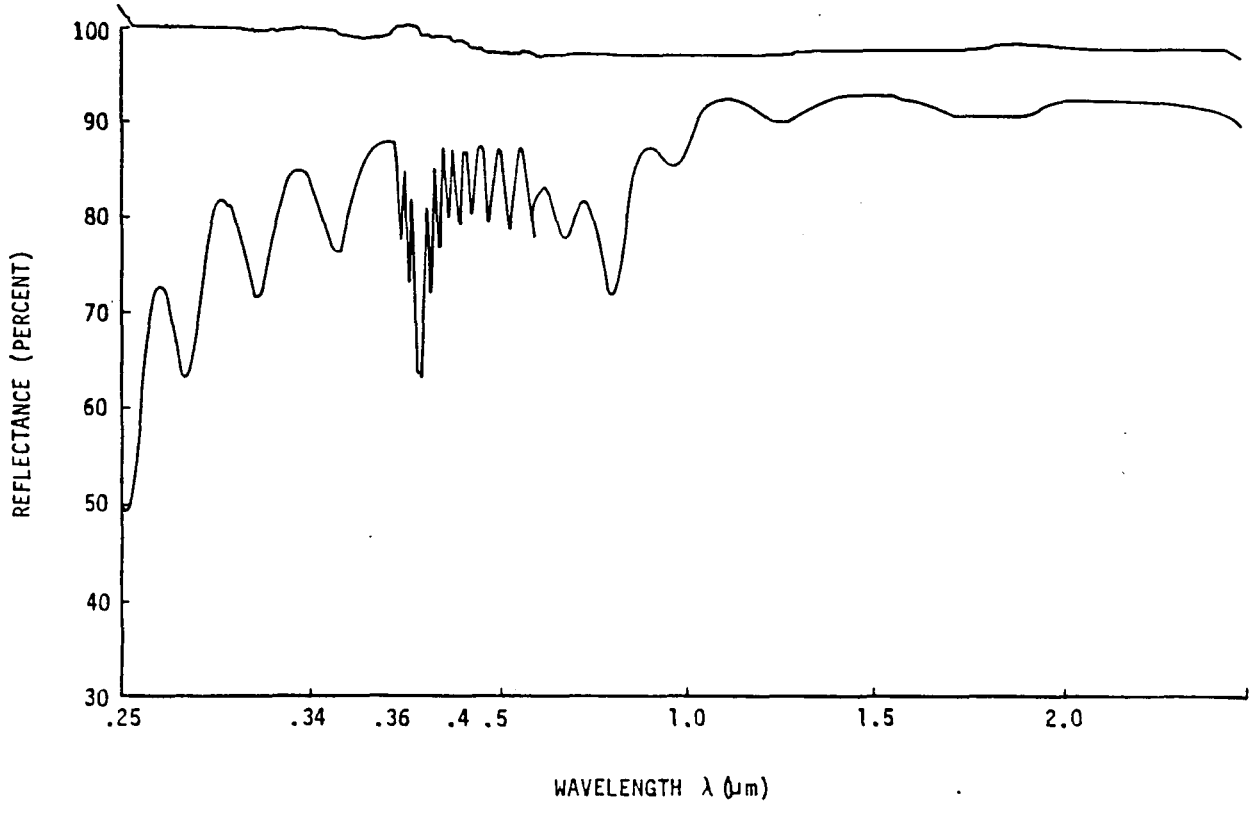

Figure 9-5. Specular Reflectance Curve Measured for SiO_x Coated Aluminum Concentrator Reflector

those reported in the table which were measured during the dry period.

It is anticipated that in the future improved substrate surfaces will be obtained with the male die and the improved optical coatings obtained with silver coatings will increase the concentrator efficiency to substantially greater than 80%.

In order to determine exact pointing error requirements, the exact cavity configuration and optical parameters must be known and coupled with the optical performance of the concentrator. This is true because the absorber/emnitter temperature depends on both concentrated sunlight absorbed and the energy absorbed from reflections back to the absorber/emitter from the cavity walls. It is also a function of the cavity window diameter. The desired absorber/emitter temperature, which is a function of cell performance parameters must also be known. Thus, it can be seen that the STPV is a complex, closely coupled system and cannot be completely segmented for analysis purposes. The final requirements cannot be determined until the final cavity design is made. The situation is further complicated by the fact that concentrated sunlight which enters the cavity by scattering off the aperture rim (thereby missing the absorber/emitter) and by scattering off the absorber/emitter surface is not necessarily all lost since the photovoltaic cell can convert this energy with 14% to 16% efficiency. Thus, a complete iterative modeling process which traces the incident solar energy through the entire system until it is converted to electricity or parasitically absorbed is required in order to precisely determine optimum concentrator pointing tolerances.

However, with the present cavity design, and the preceding concentrator measurements and analysis, it appears that a pointing error tolerance of ± 0.25 degrees would be required for the STPV system. It would be desirable to relieve the pointing requirement to a nominal ± 2 degrees tolerance value.

The ±2 degrees tolerance presents a rather difficult problem in a fast (or low f number) system such as is proposed for the STPV system. The problem is illustrated in figure 9-6. When the system is shifted off axis the focal point expands (defocusses) and shifts its location. This is a common problem for both reflective and refractive optics. In order to reduce the pointing requirements on the system while maintaining the required concentrator efficiency, a study of various modifications of the system were performed.

One proposal to relieve the accuracy requirements on the parabolic reflector is the use of an optical device placed at the aperture of the TPV cavity. Most refractive or reflective optical devices, due to the problems discussed above, cannot improve the focusing of an image once it is confused either by a nonparallel light beam or by imperfect optics elsewhere in the system such as in the parabolic reflector. However, in the case of the TPV system an optically true image is not required and it was felt that simple energy concentration enhancement might be achieved. A device which appeared promising is called an internal reflection concentrator, or light funnel, and has the potential to collect light from various singles and direct it to the bottom plane of the funnel. The funnel uses the principle of total internal reflection rather than refraction in order to direct incident light down to the concentrating plane.

A cross section of an internal reflection concentrator segment is shown in figure 9-7. In principle, light entering the front (or inner) surface of the concentrator structure is trapped by internal reflection and funneled down to the exit where a concentrated spot of hightly diffuse light results. The critical parameters are the angles θ and β. For a given θ, β must be chosen, based on the refractive index of the material so that light incident parallel to the optical axis will encounter the rear surface at an angle equal to or greater than the critical

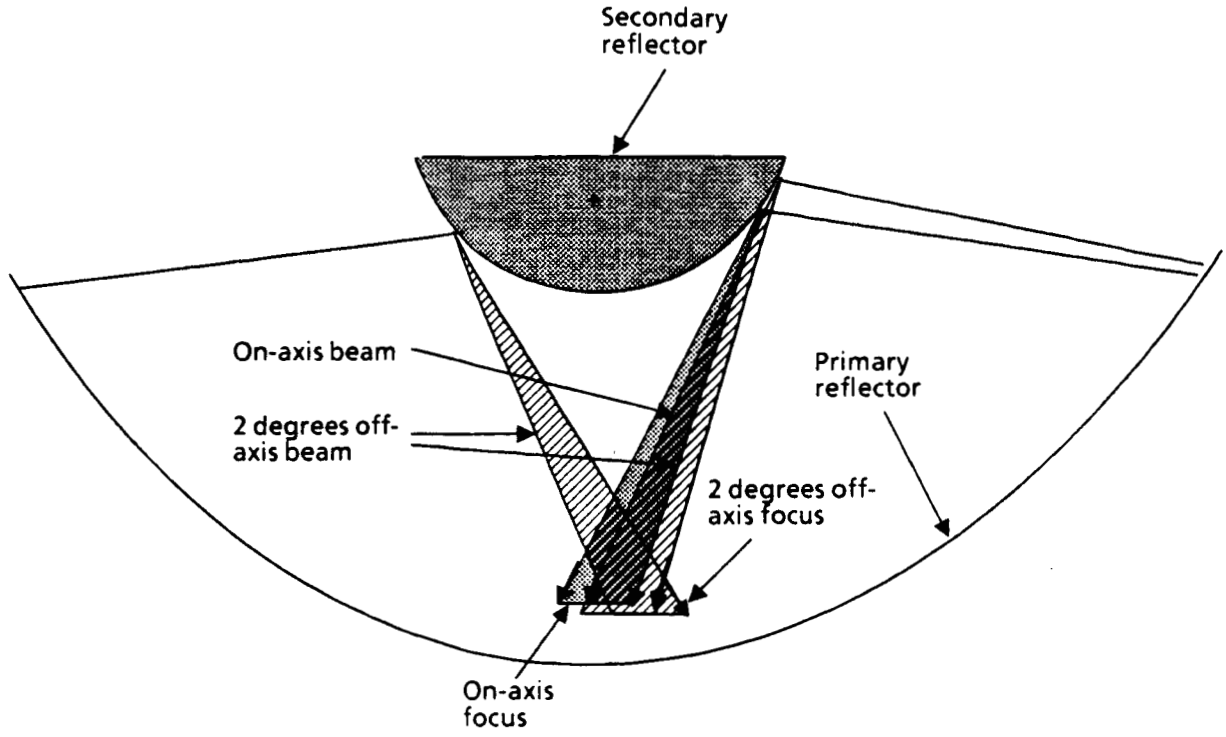

Figure 9-6. Illustration of Focal Point Shift and Expansion Due to 2 Degrees Pointing Error in Fast Cassegrainian Concentrator Optics

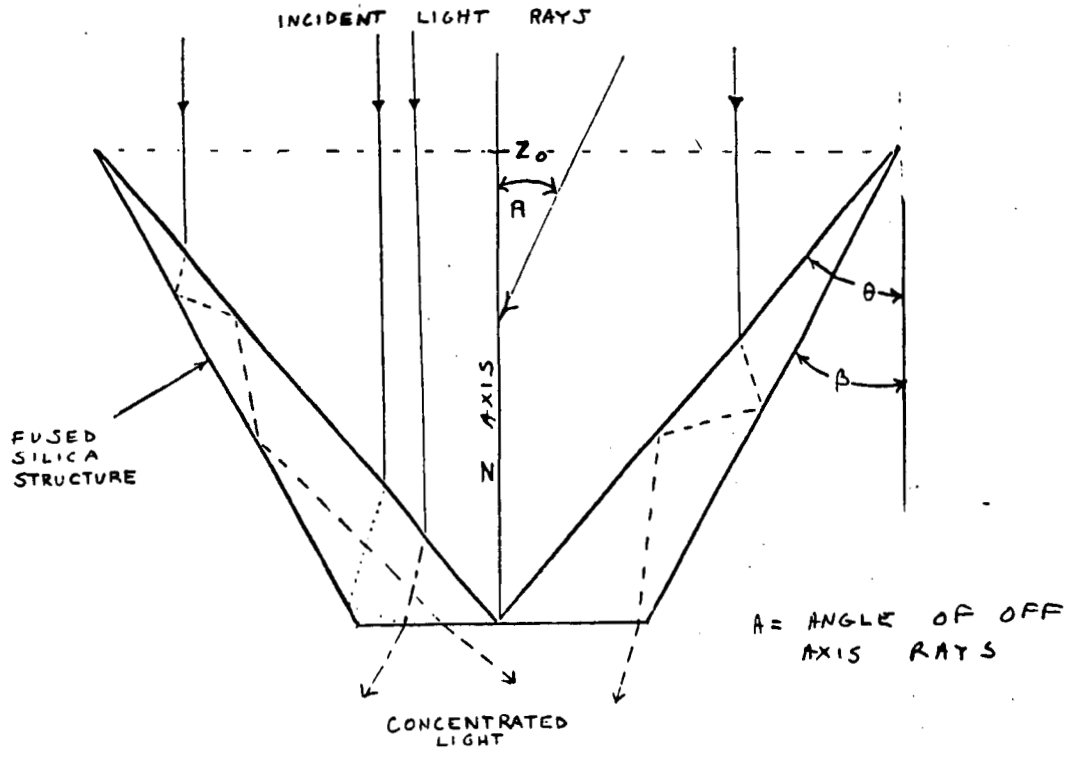

Figure 9-7. Illustration of Light Funnel Concentrator Concept

angle so that total internal reflection occurs. Each succeeding reflection then becomes farther from the critical angle allowing the light to totally reflect until it strikes the end of the funnel. This concept is very tolerant to pointing errors. Figure 9-8 illustrates its insensitivity to pointing errors of up to ± 5 degrees. This insensitivity is controlled by tolerance designed into the angle β. Because of the tolerance to pointing error, it was felt that the light funnel when placed at the cavity aperture might be a useful device for relieving the pointing requirements of the overall STPV system. The proposed configuration in which the light funnel is incorporated into the STPV system is shown in figure 9-9.

In order to analyze the system an existing three-dimensional ray-tracing code was modified to allow several configurations of light funnel to be evaluated in a TPV system. The code assumes parallel rays input at various incoming angles ranging, in the case of the TPV system, from about 5 to 20 degrees. The beam can be focused at any height above or below the aperture. The exiting rays are followed to the target plane, 0.4 in below the aperture.

The ray tracing code development started with defining the equations of the primary (1st) and secondary (2nd) surfaces of the concentrator material. The equations were then solved for the intersection of the incident ray line and the 1st surface. The angle made between this line and the normal to the surface was then found and appropriate laws of optics were applied to find the fraction of energy in the ray which was refracted into the concentrator material and the direction in-space of this refracted ray. An equation for a new line was then defined from this direction and the 1st intersection point. Then the intersection and angle of the new line and the 2nd surface was found and the angle was compared with the critical angle for internal reflection. If the angle was less than the critical angle or some reasonable fraction thereof, the ray was assumed to

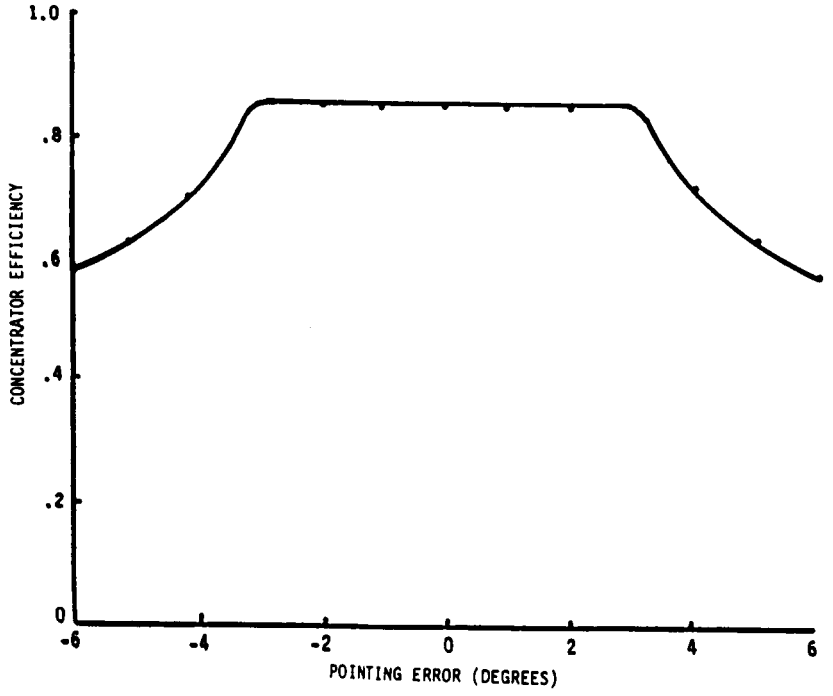

Figure 9-8. Concentrating Efficiency Versus Pointing Angle For Light Funnel Concentrator

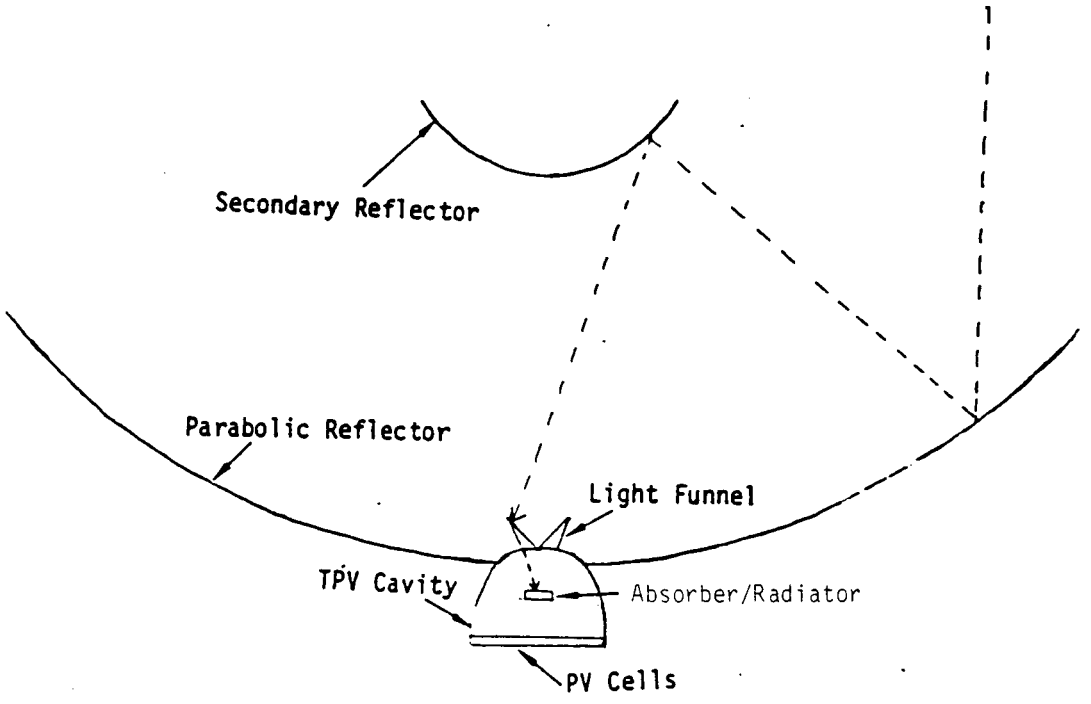

Figure 9-9. Configuration of Light Funnel Enhanced TPV Concentrator System

escape the concentrator; if not, the ray was assumed to be trapped. The above process was repeated following the ray from the 2nd surface back to the 1st and so on down to the bottom plane. The ray was then checked to see if it intersected the bottom plane at less than the critical angle. If so, it was allowed to escape the bottom plane and was traced to the target plane. The program then iteratively steps through a matrix of incident ray points at the Z0 plane until the entire concentrator is covered and desired energy total, intersection points, etc. were printed.

There are two basic ways the light funnel can collect off-angle rays. The first is to have a thick-walled funnel as shown in figure 9-10. The critical angle for trapping the light determined by the equation

$$\theta_c = \arcsin\left[\frac{1}{N}\right]$$

where n is the refractive index of the material. To find:

$$\beta = \theta - \theta_c + \arcsin\,[\sin\,(90-\theta-A)/n]$$

where θ is the angle of the inner wall, β is the angle of the outer wall, and A is the angle of incidence of the incoming rays (see fig. 9-7). It can be seen that as $\theta - \beta$ increases, A also increases, allowing rays at steeper angles to become trapped.

A second approach is to design the upper portion of the funnel to accept only a small angular offset and flatten the outer wall at the bottom in order to trap those rays which are at a greater angle of incidence (as shown in fig. 9-11). In both cases, the original assumption was that the beam was focused directly on the aperture and hence on the bottom of the funnel. The upper radius of the funnel must be large enough to accept the entire incoming beam at the maximum expected angle of incidence.

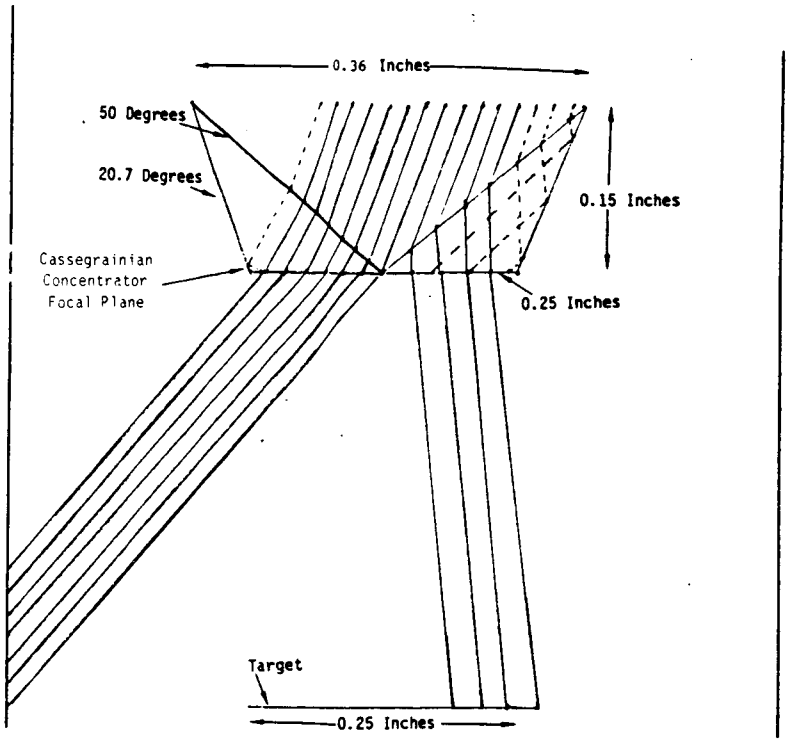

Figure 9-10. Progression of Rays Through Thick Walled Light Funnel

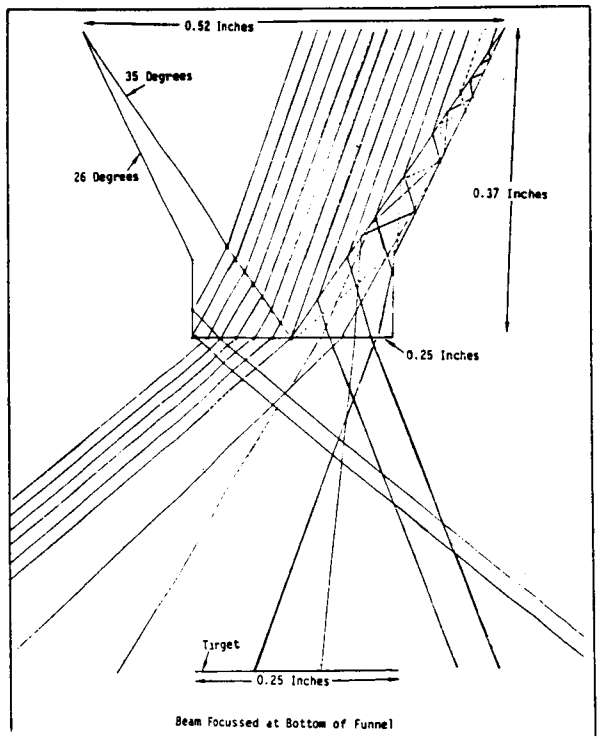

Figure 9-11. Progression of Rays Through Flattened Outer Wall Light Funnel

An example of the actual progression of the rays through a plane of the first type of funnel can be seen in figures 9-10 and 9-11. The plane of view is parallel to the incoming rays. The rays depicted by a dashed line hit the bottom plane at greater than the critical angle and are therefore trapped in the funnel. For this particular configuration, figures 9-12 and 9-13 show a plot of the rays which reach the target plane at both 10 and 20 degree angles of incidence. At a 20 degree angle of incidence, 3.5% of the rays are trapped. Of the remaining rays, most leave the bottom at a great enough angle to miss the absorber/emitter target. Only 4% of the original rays reach the target.

Several approachs (approximately 100 configurations) were analyzed in an attempt to solve the problems mentioned above. The beam was refocused at various planes and the inner surface was raised above the bottom plane. Basically it was found that the diffuse angles of the rays exiting from the light funnel base limited its usefulness, although several configurations did come close to solving the problem.

It was found that a combination of the light funnel concept and reflective optics was required in order to adequately relieve the pointing requirements to ± 2 degrees without undue degradation of the concentrator performance. Figure 9-14 shows a configuration of the light funnel incorporating an external reflective surface. The outer angle of the surface was chosen so that only those rays hitting the funnel at an angle to the normal of $90-\theta+A$ are captured. Those hitting the opposite surface pass through the funnel and either continue down to the target plane or bounce off the external reflector. The reflector angle was chosen so that rays incoming at 20 degrees or more off the optical axis will reenter the outside funnel wall and be internally reflected from the internal wall, continuing to the bottom plane. The depth of the reflector was determined by the outer most rays which escape the funnel and hit the target. All others must bounce off the reflector in order to reach the target. This configuration is

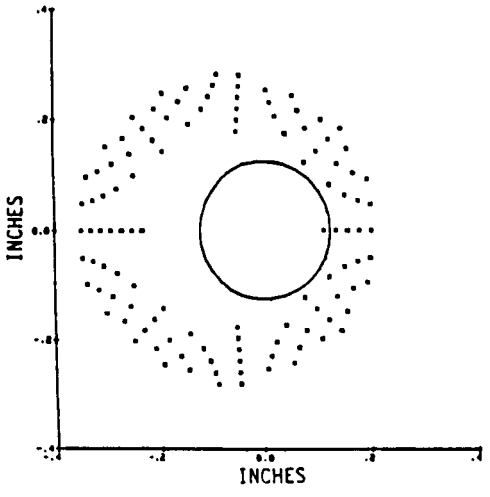

Figure 9-12. Plot of Rays Hitting Target Plane Angle of Incidence -10 Degrees 2% of Rays Hit Target

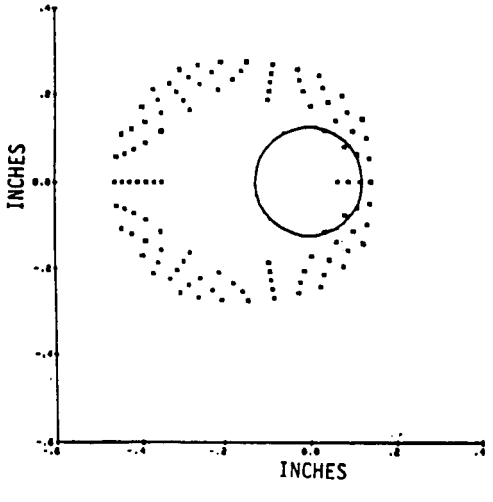

Figure 9-13. Plot of Rays Hitting Target Plane Angle of Incidence -20 Degrees 4% of Rays Hit Target

highly successful for on-axis use and deteriorates very slowly as the off axis angle increases. Table 9-2 summarizes an analysis of the average percentage of rays escaping from the funnel both as a function of off-axis angle and as a function of point of origin on the primary reflector.

When one performs such an analysis for the entire reflector, the rays coming from the side of the primary that is tilting away from the sun (designated as a + error angle in the analysis) are captured more efficiently than those originating from the side tilting toward the sun. Table 9-2 summarizes those rays originating from the side tilting toward the sun. Thus, if one considers that the rays from the rest of the reflector are captured more efficiently, then it appears that the STPV can be made tolerant to ± 2 degrees off-axis pointing error with less than 90% loss in concentration efficiency onto the absorber/emitter. If one considers that the 10% or less of the energy that misses the absorber/emitter, the photovoltaic cell in the cavity can still convert it with ~15% efficiency, then the overall pointing error degradation of efficiency is on the order of 5% to 7%. (A more thorough analysis of the overall integrated collection efficiency is continuing and will be included in the final report.)

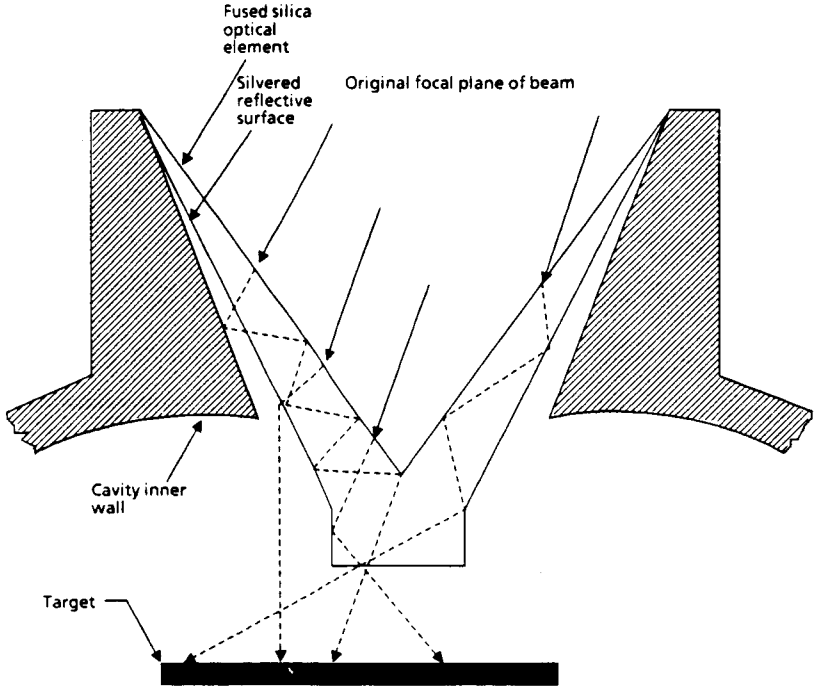

Figure 9-14. Illustration of the Optical Configuration Used to Relieve Pointing Tolerances on STPV System (With Beam on Axis)

Table 9-2. Summary of Collection Efficiency For "Worst Case" Rays as a Function of Pointing Error

Pointing error	Collection efficiency as a function of radial position on primary reflector 2"	3"	4"	5"
0°	100.0%	98.9%	90.4%	92.1%
-0.5°	92.7%	87.6%	87.6%	87.0%
-1.2°	85.9%	87.6%	89.3%	81.9%
-2.0°	81.9%	87.6%	89.3%	81.9%
+ 2.0°	100.0%	100.0%	97.2%	95.3%

10.0 THERMAL CONTROL SYSTEM

Even with a 30% system conversion efficiency, the waste heat that must be radiated back to space is substantial. The STPV module accomplishes this by utilizing the concentrator primary reflector in a dual role as thermal radiator. The reflective side of the primary is overcoated with SiO_x or $A_1 2_0 3$ to increase its 325°C emittance to approximately 0.45. The back surface is coated with black epoxy paint such as NEXEL in order to give it an emittance of approximately 0.90. The thermal energy is distributed over the radiator by means of six heat pipes which extend radially outward from the cavity base as indicated in the diagram of figure 1-2. The heat pipes are 5-in long, 3/16-in diameter, ammonia charged stainless steel units fabricated by Hughes Electron-Dynamics. The heat pipes are bonded to the reflector/radiator with silver loaded epoxy as shown in the photograph of figure 10-1b.

a) Diagram Of Thermal Control System

b) Heat Pipe Thermal Control System

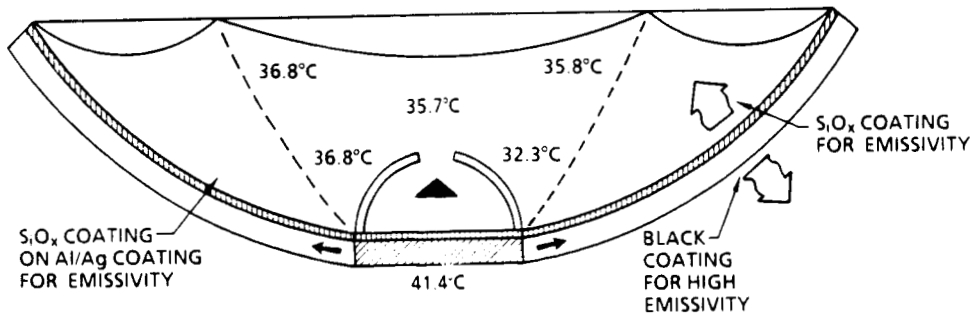

c) Thermal Vacum Test Fixture

Figure 10-1 STPV Module Thermal Control

After the heat pipes were bonded and the black NEXEL coating applied, an array of seven elements were mounted in a thermal vacuum chamber with black, LN_2 cooled walls for test as shown in figure 10-1a. Figure 10-2 shows the array mounted in the thermal vacuum chamber and fully illuminated by a close matched AMO solar simulator. The large solar simulator required to fully illuminate the array had a divergence angle of ± 2 degrees so that the energy could not be focused into a TPV cavity. Therefore, the absorptance of the cavity was simulated by a flat absorbing base with reflective areas adjusted to limit the thermal input into the system to exactly the same heat flux that would be incident on the base of an operating STPV cavity. These absorbing bases can be seen in the photograph of figure 10-3. Thus, the energy into the cavity base was the same for thermal purposes as that of an actual operating TPV cavity. The resulting radiator temperatures as measured by thermocouples bonded to the radiator surface are indicated on the diagram of figure 10-1c. The results are quite uniform and the base temperature of 41.4°C indicates that the photovoltaic cell temperature will be kept below 50°C during operation. These measured temperatures agreed well with predictions made by thermal analysis. The system was then thermal cycled between -100°C and +80°C in the thermal vacuum chamber. The coatings survived the thermal cycling tests. At the end of the test the solar simulator was shut down and the assembly cooled down to near LN_2 temperature. Some of the coatings delaminated at near LN_2 temperature; however, this is well below the expected operating temperature.

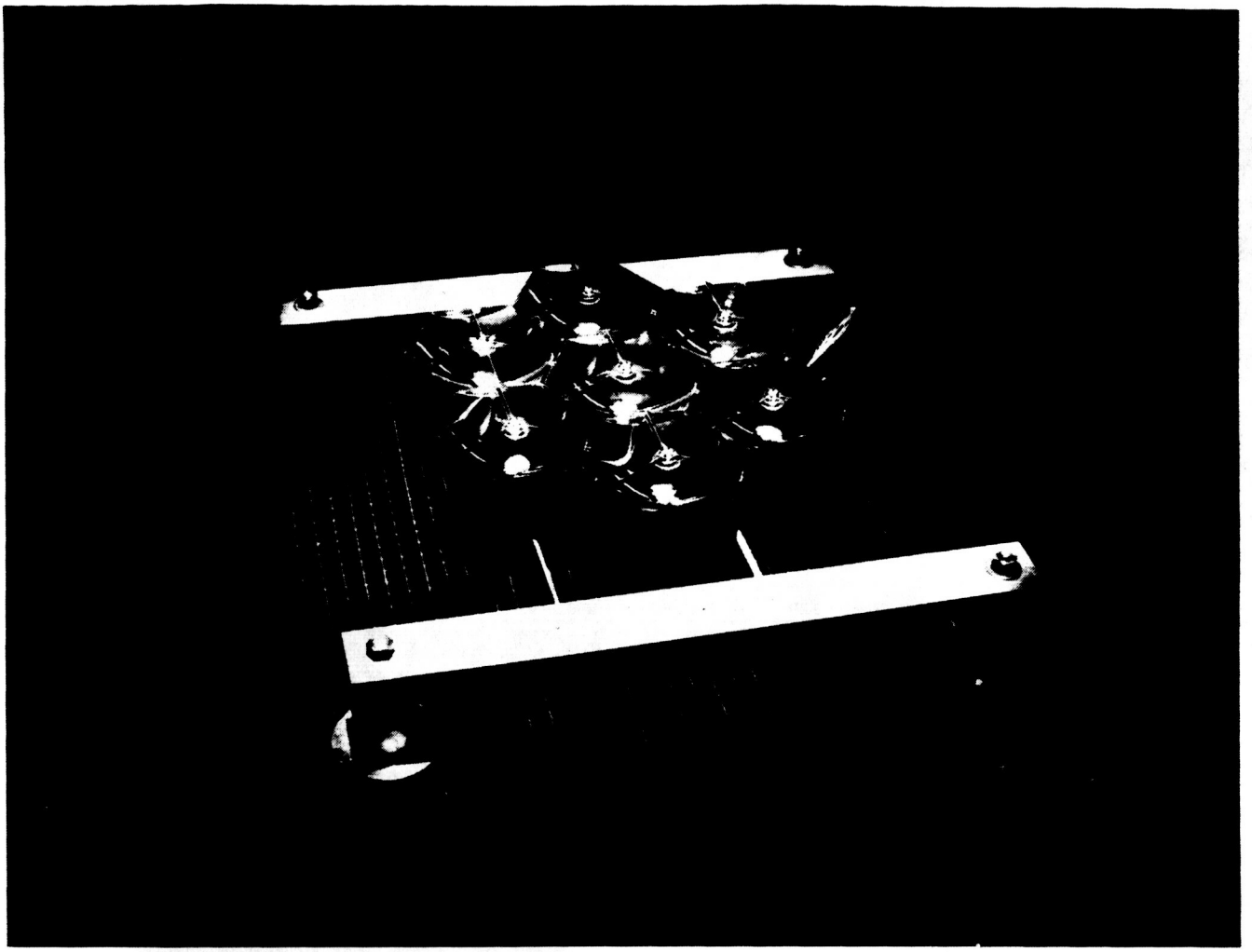

Figure 10-2. Photo of STPV Concentrator Array Mounted in Thermal Vacum Test Chamber

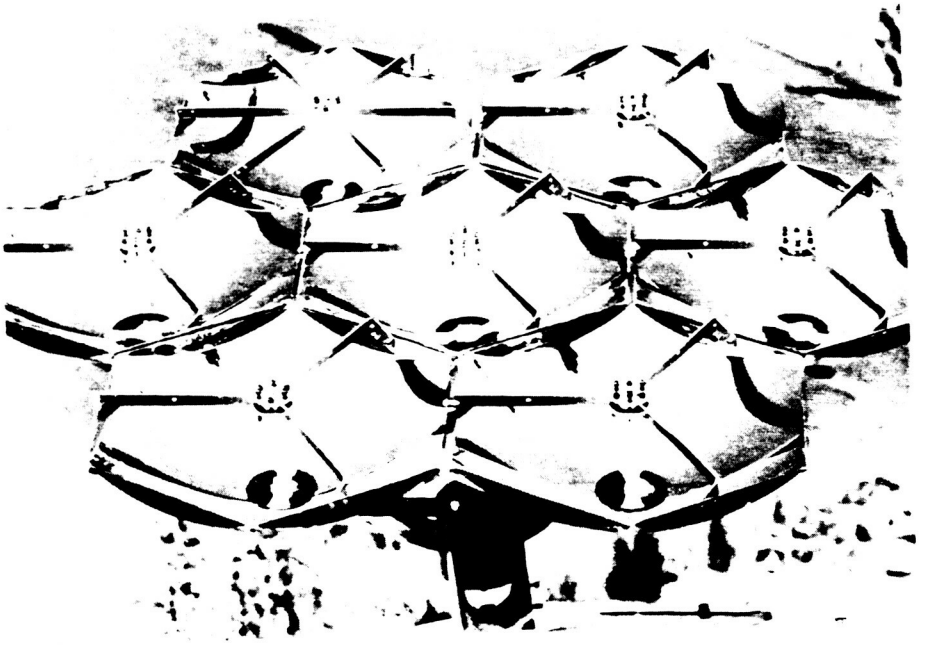

Figure10-3. Photo of TPV Concentrator Optics

Thus, the effectiveness of the thermal control system has been demonstrated and it appears entirely adequate for the STPV system; however, the heat pipes are heavy, expensive components. An analysis of the weights of the TPV system components was made and it was determined that the heat pipes were a significant weight factor in the design. The results of this analysis are summarized in table 10-1. The heat pipes constituted 23.5% of the laboratory prototype by actual weight. They represented 54% of the estimated weight of an optimized production module. The heat pipe weight cannot be reduced because it is controlled by the wall thickness required to withstand the pressure of the working fluid. Further, the heat pipes also constitute the largest cost item in the design representing about 70% of the module cost. They also carry a considerable reliability penalty with them. For the above reasons, a thermal analysis was performed to see if the heat pipes could be eliminated. This study was further indicated by a previous observation that cells operating in an STPV cavity have only about one-third the temperature coefficient of cells exposed directly to AMO sunlight. This is true because the TPV photocell is operating on the leading edge of the blackbody emitted energy distribution curve. As its bandgap narrows with increasing temperature it converts more of the incident spectrum to electron-hole pairs. As a result, the increase in short circuit current offsets the decrease in voltage with increasing temperature. Measurements of these effects are shown in figure 10-4.

Table 10-1. Weight of 10-inch TPV Module

	Measured Values for Boeing Prototype Model	Easily Achievable	Achievable in Production
Primary	63 gm	40 gm	20 gm
Secondary	17 gm	12 gm	2 gm
Cell Cavity	24 gm	19 gm	5 gm
Heat Pipes	32 gm	32 gm	32 gm
Total Weight:	136 gm	103 gm	59 gm

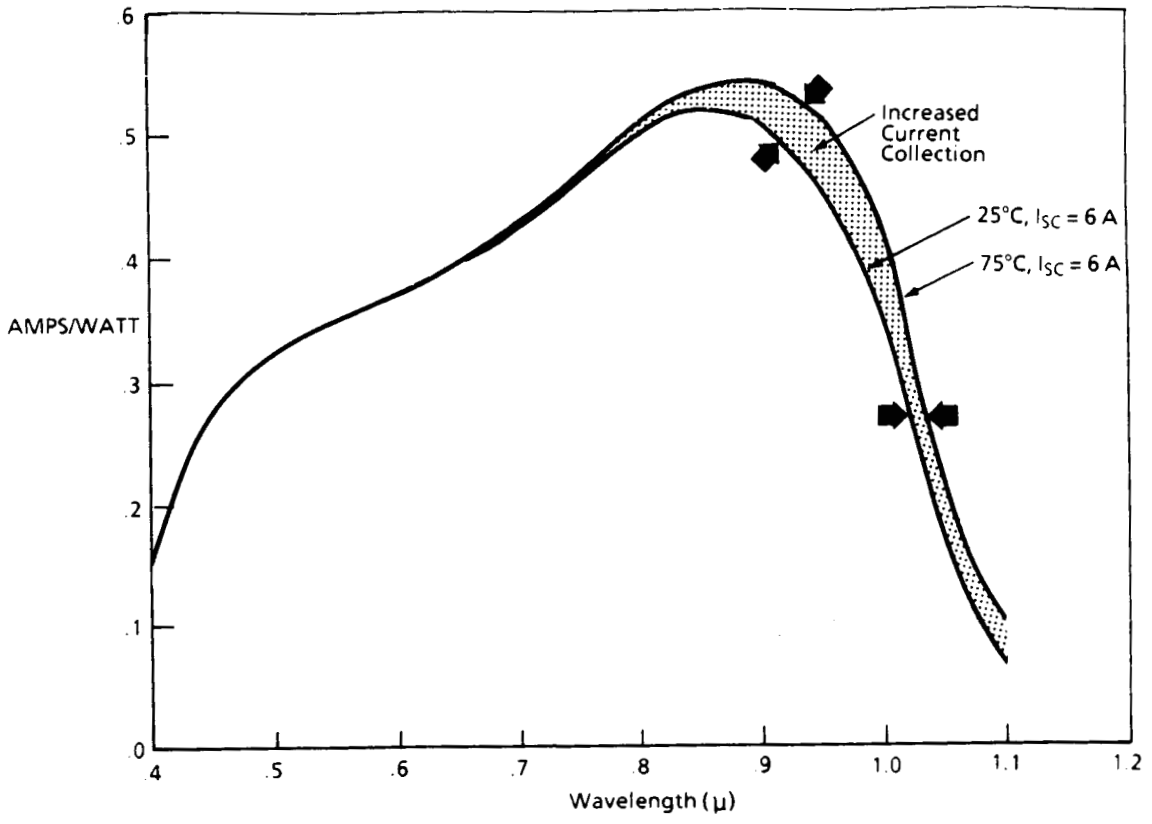

Figure 10-4. ASE 8-mil TPV Cell: External Response VS. Injection, Temperature

Thus, by considering these effects in the STPV model, it appears that for a silicon cell the STPV efficiency temperature coefficient is approximately one-third that of a silicon cell exposed to the space sunlight spectrum. For GaAs the STPV is virtually independent of temperature over a wide range. Figure 10-5 illustrates the relative temperature coefficients for conversion efficiency. From these observations it is evident that in the TPV cavity the photovoltaic cell can be allowed to operate at a significantly higher temperature than 45°C. Thus, it appeared that the heat pipes might not be required to distribute the heat from the cavity base to the radiator. Rather, one could design for thermal conduction to distribute the heat by allowing the cell temperature to increase.

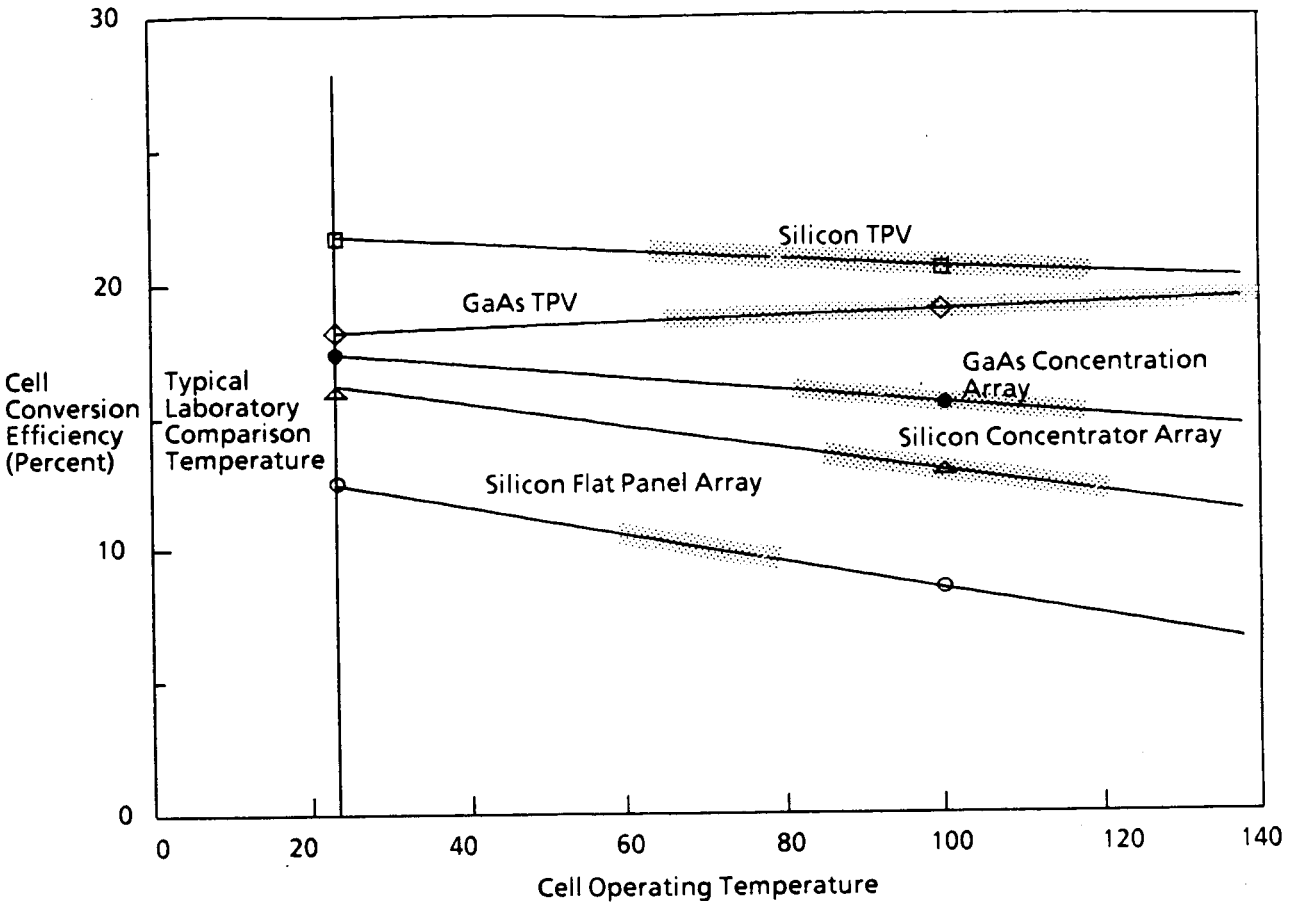

Figure 10-5. Comparison of Operating Efficiencies for TPV System Versus AMO Panels

The new upper temperature is assumed to be 100°C. The object of the thermal study was to determine whether the increased temperature tolerance would eliminate the need for the use of heat pipes. The study shows that the heat pipes may be eliminated and the operating temperature may not need to be as high as 100°C depending on the material used for the primary reflector/radiator.

In order to perform the thermal analysis the Boeing Engineering Thermal Analyzer (BETA) code was used. The BETA code is a general program for the solution of heat transfer problems. The system under consideration must first be broken down into a system of discrete nodal volumes. The mass of each volume is "lumped" at a point or "node" within the volume, and the paths for the conduction of heat from one node to another is represented by conductors (conduction, convection and/or radiation) connecting the appropriate nodes.

The BETA code solves the network system using an iterative numerical method. Given a network with temperatures known at each node, this method predicts a new value of the temperature at each node, one iteration later. The process of predicting new temperatures from old temperatures is repeated for many iterations until the problem is completed at the end of a specific time interval or when steady-state is reached.

For purposes of thermal modeling, the primary reflector was approximated by a disk of the same radius. The effective area of the front of the parabolic surface is exactly a disk while the effective back area is about 20% larger. Therefore, a disk approximation is a conservative approach. To approximate the actual module, the disk is assumed to be 10 inches in diameter, 20 mils thick, and composed of magnesium. All surface coatings were neglected. The cell radius was 0.7 in.

The system operates at 30% efficiency, with an incident energy of 1 sun over the area of the primary reflector or a flux of 0.3 sun is converted to usable energy. About 15% of the incident energy will be absorbed by the surface of the primary reflector, as shown by the reflectance data in figure 10-6. About 15% of the remaining energy will be absorbed by the secondary reflector. So the total energy (power, actually) to be dissipated by the system is (1.0 - 0.3 - 0.85 x 0.15) sun x A_p* = 0.5725 sun x A_p, with 0.15 sun x A_p distributed evenly over the reflector surface and 0.4225 sun x A_p absorbed by the cavity base in the area below the cell.

The front surface emissivity, E_1, is assumed to be 0.45 as indicated by the data in figure 10-7, and the back surface emissivity, E_2, is 0.9. To determine the initial temperature (average steady-state temperature) the following equation was used:

*Where A_p = area of the primary reflector.

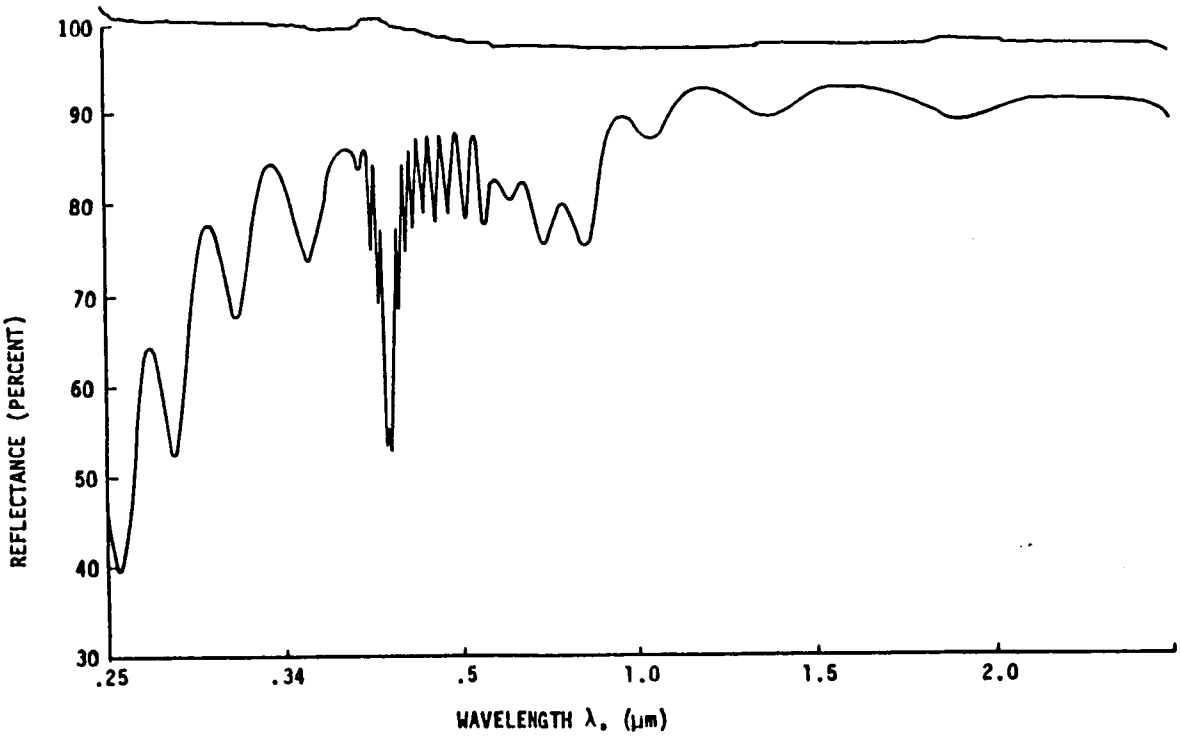

Figure 10-6. *Unirradiated Reflectance Curve for A1-Si0$_x$ Coating (Total Solar Reflectance ~ 88 Percent)*

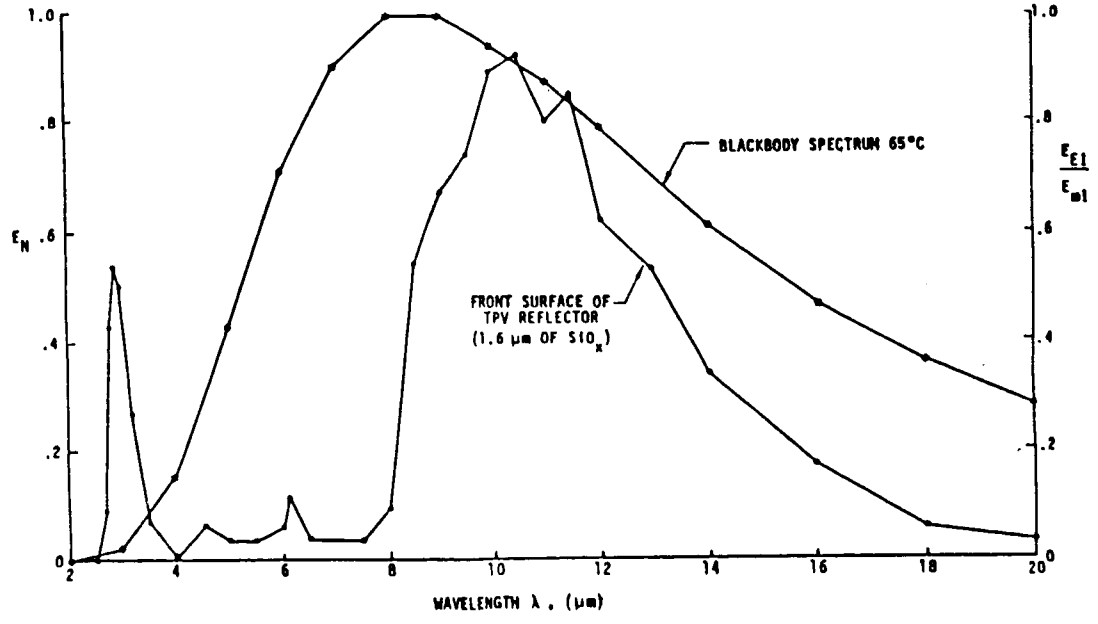

Figure 10-7. *Comparison of Al-Si0$_x$ Coating Specular Emittance to Blackbody Spectrum at Operating Temperature (Total hemispherical Emittance = 0.45)*

$$P = (E_1 + E_2)\ A_p\ \sigma\ T^4$$

where P is the power to be dissipated (0.5725 sun x A), E_1 is the front surface emissivity, E_2 is the back surface emissivity, A is the area of the disk, σ is the Stefan-Boltzmann constant (5.68E-12), and T is the absolute temperature. This gives an initial temperature of 317.6 K.

Due to the radial symmetry of this problem a two dimensional network was chosen. Figure 10-8 shows the network used. The mass of each ring of constant change in radius is lumped at each node. Volumes used are for an entire ring. Nodes on the top and bottom surface have a value of zero. This is to allow a heat flux to be specified at the surface of the material and is called a π mesh or Neumann boundary condition. The flux for this problem is the radiated energy from the front and back surfaces. All energy is assumed to be deposited in the inner nodes.

The BETA code results for a 20-mil thick magnesium disk are shown in figure 10-9 which is a plot of the steady-state temperature versus radius across the disk. Figure 10-10 is the same plot for a 40-mil thick disk. The maximum allowable temperature at the cell is 100°C or 373 K, so the 20-mil disk does not dissipate enough heat. The 40-mil disk will keep the temperature down, but is undesirable because of its increased weight. An alternative solution is to make the disk 40 mils thick in the center, gradually decreasing to 20 mils thick at the outer edge. The results of this configuration are shown in figure 10-11.

Another possibility for better heat dissipation is to use a material other than magnesium. Aluminum or beryllia may be better choices for this application. Both have higher thermal conductivity than magnesium and are castable in molds which would permit precise dimensional control. The properties of magnesium, aluminum and beryllia are compared in table 10-2.

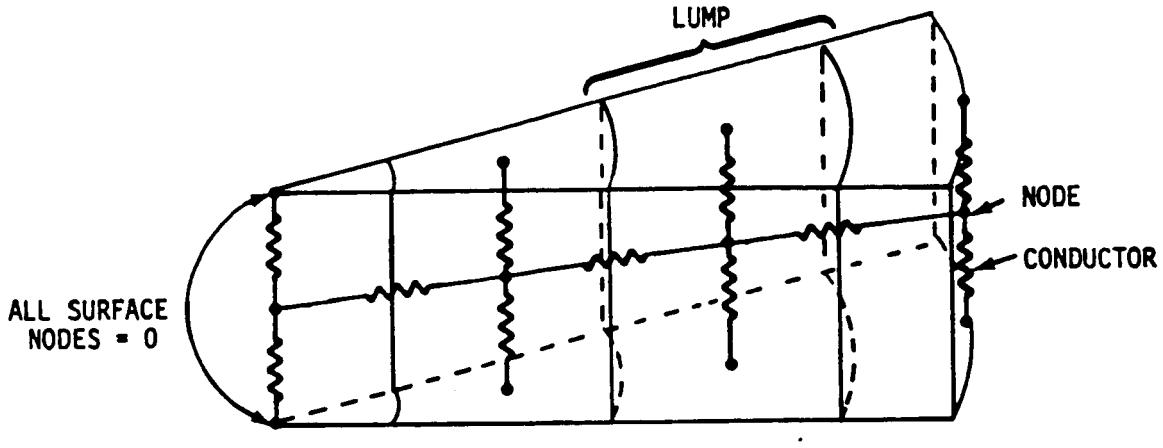

Figure 10-8. Network System for Beta Code Analysis of TPV System

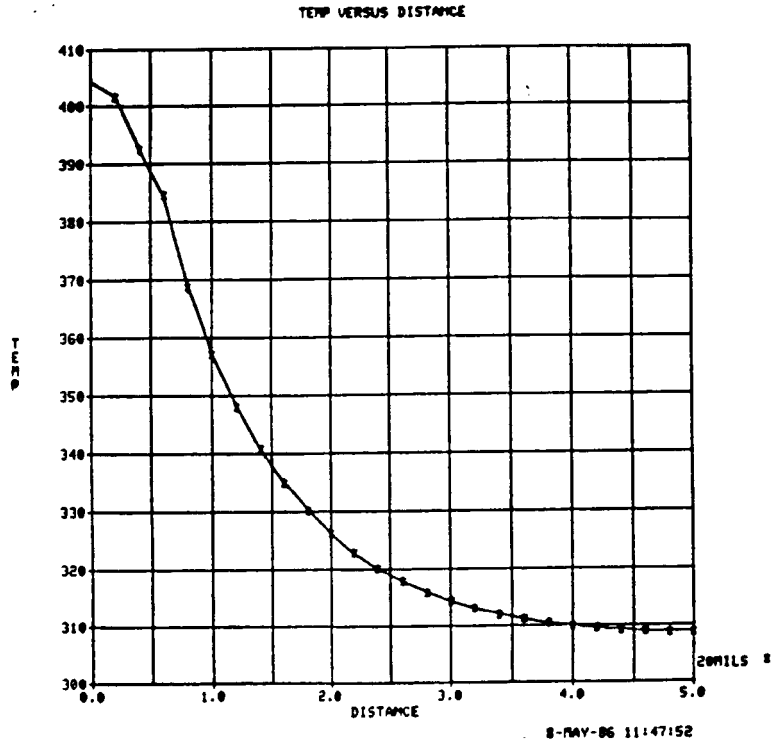

Figure 10-9. Steady-State Temperature Versus Radius of 20-mil Disk

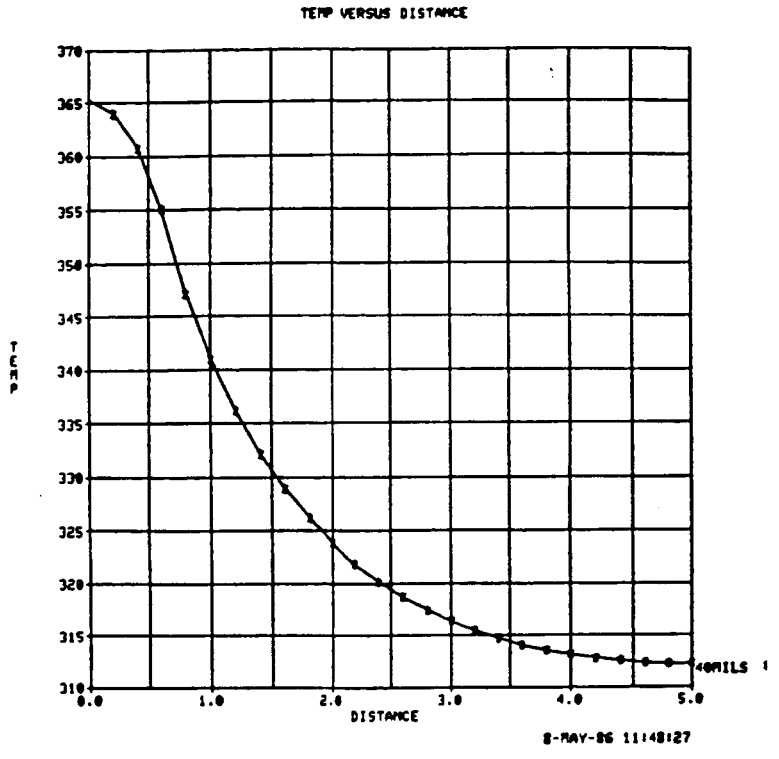

Figure 10-10. Steady-State Temperature Versus Radius of 40-mil Disk

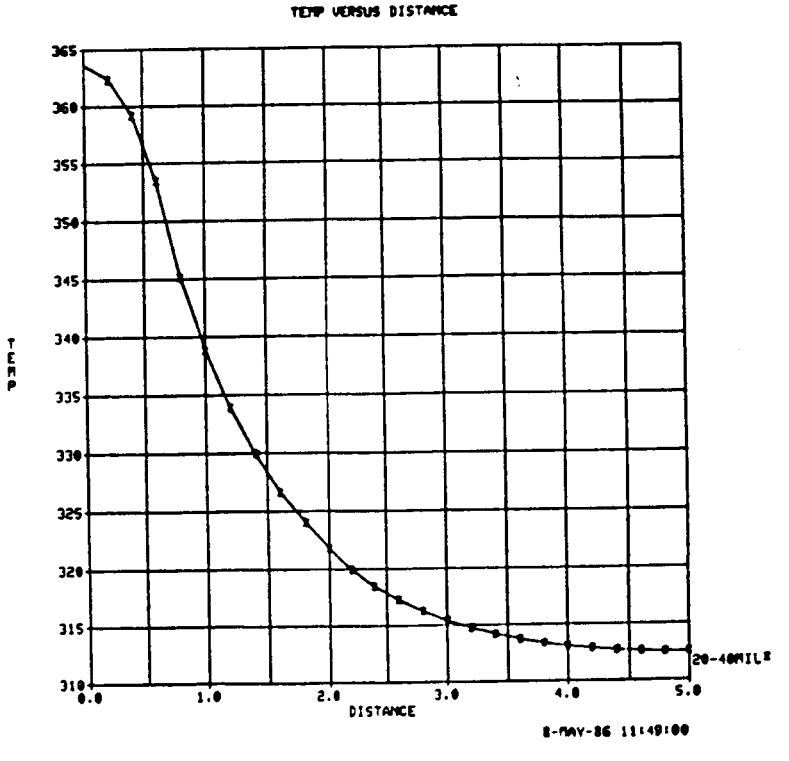

Figure10-11. Steady-State Temperature Versus Radius, in 40mil Disk Tapering to 20 mils at Outer Edge

Table 10-2. Comparison of Material Properties

	Magnesium	Aluminum	Beryllia
Density	1.74 gm/cm^3	2.7 gm/cm^3	2.88 gm/cm^3
Thermal Conductivity	1.530 W/cm-deg	2.40 W/cm-deg	2.51 $\frac{\text{cal-cm}}{\text{cm}^2\text{-sec-}^\circ\text{C}}$
Specific Heat	0.1307 cal/gm°C	0.230 cal/gm°C	0.53 cal/gm°C

Analyses similar to that for the magnesium radiator indicates that 25 mils tapering to 13 mils of either aluminum or beryllia would provide the necessary thermal conductance resulting in cell temperature of 100°C. The relative weights of a 24 mil magnesium primary reflector such as that used in the Boeing model and 10 mil aluminum and magnesium primaries are 28 gms, 28.7 gms, and 30.6 gms respectively. Thus, it can be seen that not only can the weight of the heat pipes be eliminated, but the resulting primaries can be equivalent in weight to the magnesium primary.

Thus, because of their better properties as a substrate material, it is recommended that either aluminum or beryllia be used as the primary reflector substrate material. Beryllia, being a hard material would provide the best substrate surface; however, aluminum is much more economical and easier to work with. Both these materials should be examined experimentally and the best candidate chosen based on a consideration of performance and production cost.

11.0 OPTIMUM SPACE MODULE DESIGN

There are many factors to consider in optimizing the STPV design. These factors include performance, weight, launch or storage volume, deployment, cost, and producibility. In the previous design effort the size of 10 inches from vertex to vertex for the primary reflector was chosen as a compromize between heat pipe length and minimum size of cavity for producibility. The weight of the system increased roughly as the square of the heat pipe length. Therefore, one wanted to keep the pipes as short as possible. However, due to the requirements for thermally suspending the absorber/emitter on delicate wires that are small compared to the absorber/emitter of 0.25 inch diameter appeared to be the smallest practical size. These considerations combined with the focal spot size of the cassegrainian system determined the 10 inches reflector size.

Launch volume considerations led to the placing of the secondary mirror in the plane of the rim angle of the primary reflector. This configuration gave a flat panel 2.5 inches thick that could be stored and deployed as depicted in figure 11-1.

The current design will not use heat pipes. Rather, it will allow the cell to operate at 100°C and rely on thermal conduction to remove the heat from the cell and transport it to the radiator surface. However, it appears that 10 inches may again be the optimum size. The elimination of heat pipes does not change the factors that led to the 10 inch module being the smallest practical module size. The larger the primary, the deeper, or thicker, the panel must be. The launch volume suffers if the size is increased due to the deeper panel. Further, since more heat is generated in the cell by a larger primary, then the primary must be thicker in order to conduct the heat array. Thus the system weight increases approximately linearly with primary reflector size. The performance of the system is not enhanced by

larger size. These types of considerations have led to the decision to retain the 10 inch size module.

However, several design changes are recommended in order to optimize the module performance and producibility. First, with the blow forming process, considerable difficulty was encountered due to crystallization of the material during the forming process. The folded up sides on the hexagonal facets of the reflector (as was shown in the photograph of fig. 9-1) were convenient for stiffening the reflector and joining adjacent reflectors; however, they made it impossible to machine polish the primary surface. Thus, in order to overcome the granularity produced by the recrystallization of the material during forming, an alkyd melamine coating was applied to make a specular substrate on which to deposit the aluminum and SiO_x to form the reflective surface. The alkyd melamine coating on the relatively complicated primary structure does not appear to be an easily producible item. For this reason it is recommended that the primary reflector be cast from a very hard aluminum alloy in order to facilitate machine polishing. Instead of the hexagonal facets being folded up as they were in the blow forming, they should be folded down as shown in the perspective drawing of figure 11-2 so that they do not interfere with machine polishing. Six webbings running from the vertexes to the center are located on the backside of the reflector. These webbings and the folded down facets serve to stiffen the unit. They are relieved by holes to reduce overall weight. A cross-sectional view of the unit is shown in figure 11-3. The cross-sectional view shows the varying thickness of the reflector which ranges from 0.0265 inch to 0.013 inch. This variable thickness facilitates thermal conduction of heat from the base to the reflector/radiator surface. Figures 11-4 and 11-5 show dimensioned plan views of the front and back of the reflectors.

The advantage of this design over the blow formed one is that the downward folded facets serve the same stiffening function yet

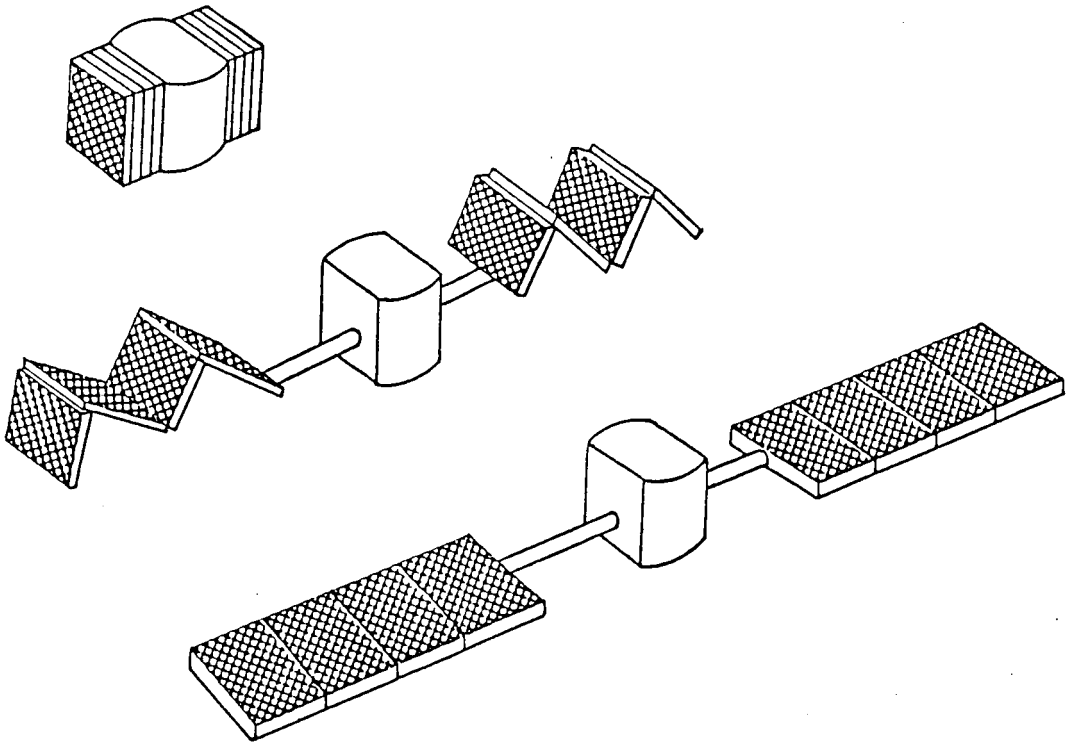

Figure 11-1. Launch and Deployment Configuration for TPV Panels

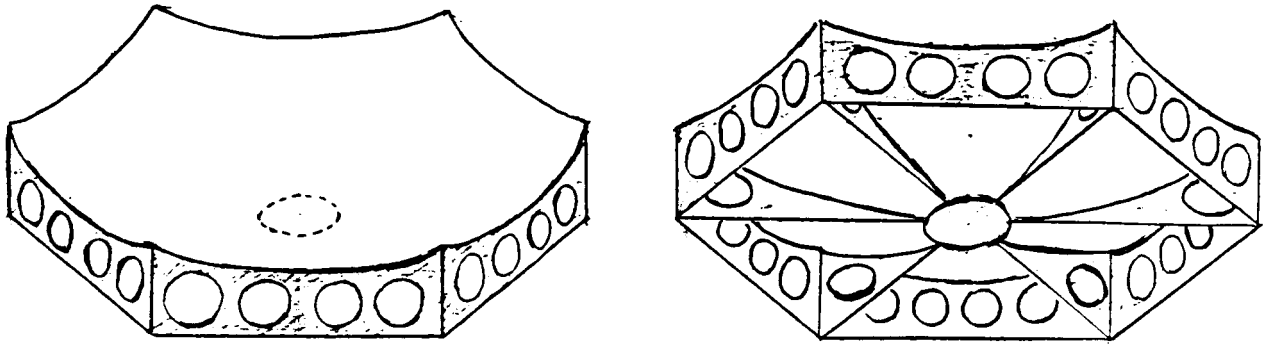

Figure 11-2. Perspective Views of Primary Reflector

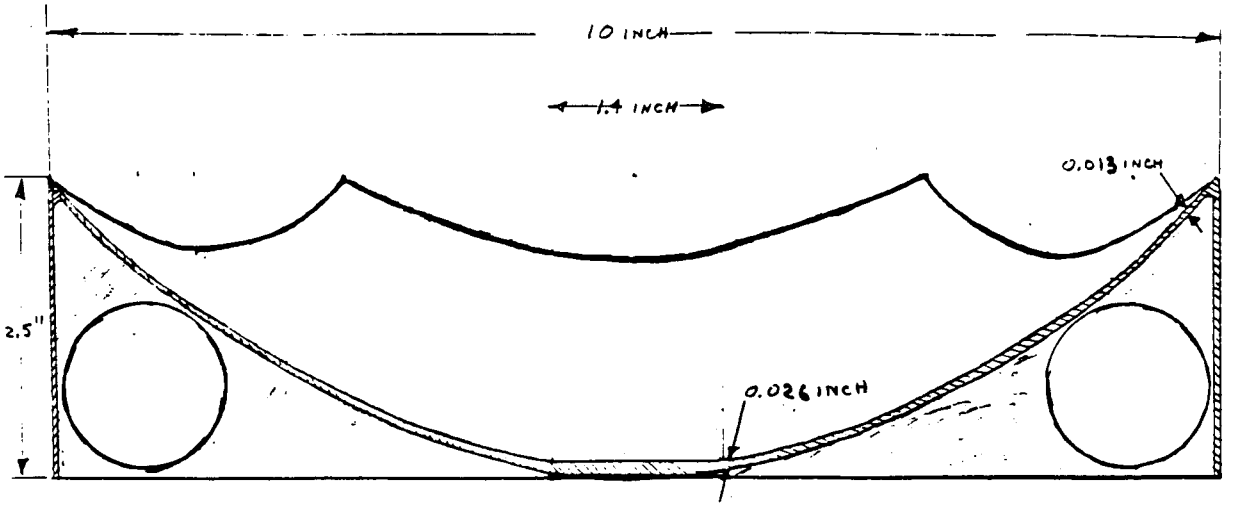

Figure 11-3. Cross-Sectional View of Primary Reflector

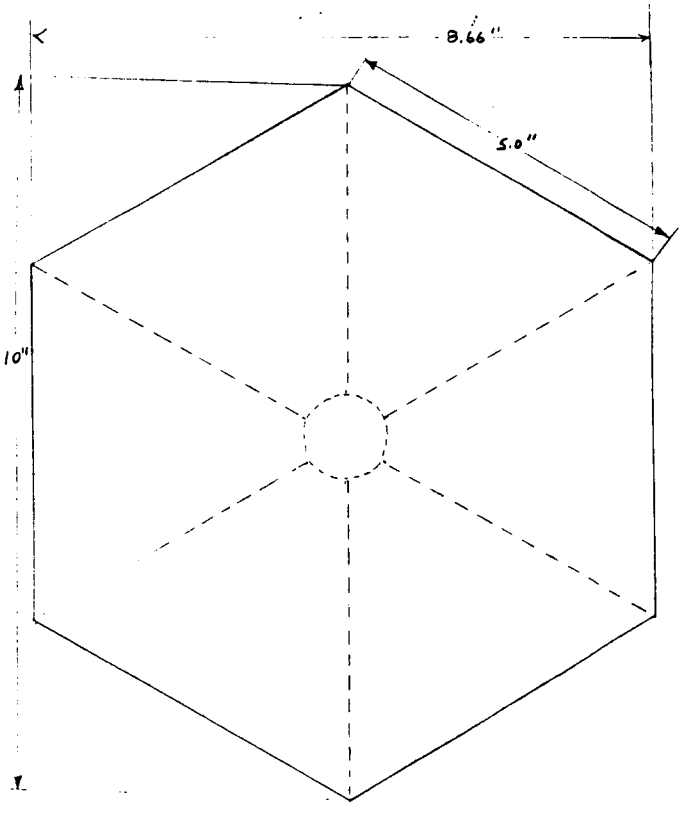

Figure 11-4. Top Plan View of Primary Reflector

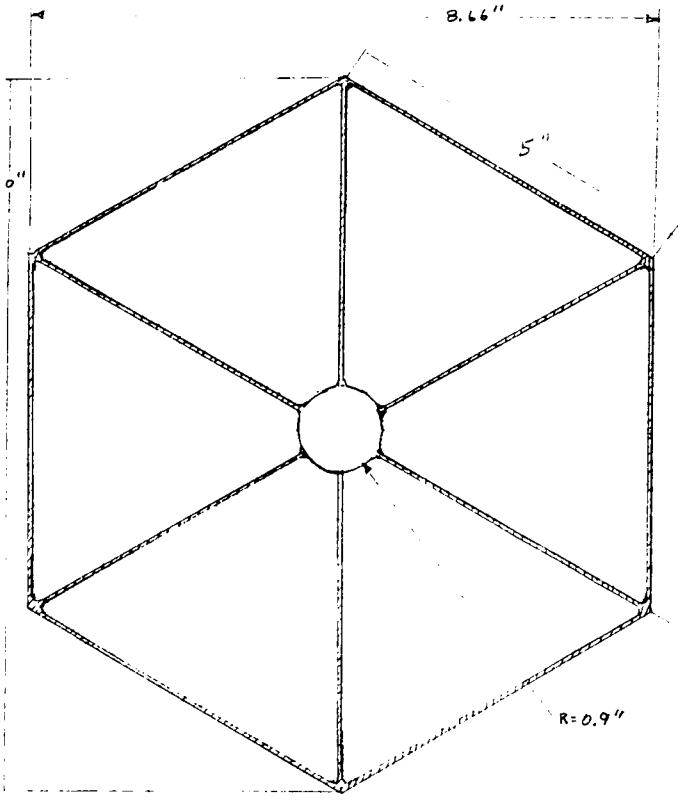

Figure 11-5. Bottom View of Primary Reflector

permit machine polishing of the reflector substrate surface. Thus, the necessity for coating such as alkyd melamine are unnecessary in order to get specularity. The use of thermal conduction to distribute heat also eliminates six heat pipes which were expensive items (approximately $200 each) and presented reliability problems. Figure 11-6 shows a cross-section of an assembly drawing of the proposed STPV module. The secondary reflector is suspended by six supports which extend radially to each facet where they are attached to the stiffener webbings. The optical enhancer is a fused silica structure which relieves the pointing tolerance of the system to ± 2 degrees. This device was discussed in detail in section 9.0.

This tolerance to pointing error greatly relieves stresses on panel and deployment mechanism design. Figure 11-7 shows how the hexagonal modules are assembled into a close-packed array to minimize light losses. A potential panel configuration is shown in figure 11-8.

A cost study was performed on the STPV system during an earlier phase. The results of the study are indicated in figure 11-9. This study is conservative for the present design in that the heat pipes which were a major materials cost factor have now been eliminated. Thus it is felt that the system has an excellent change of meeting the $20/W cost figure.

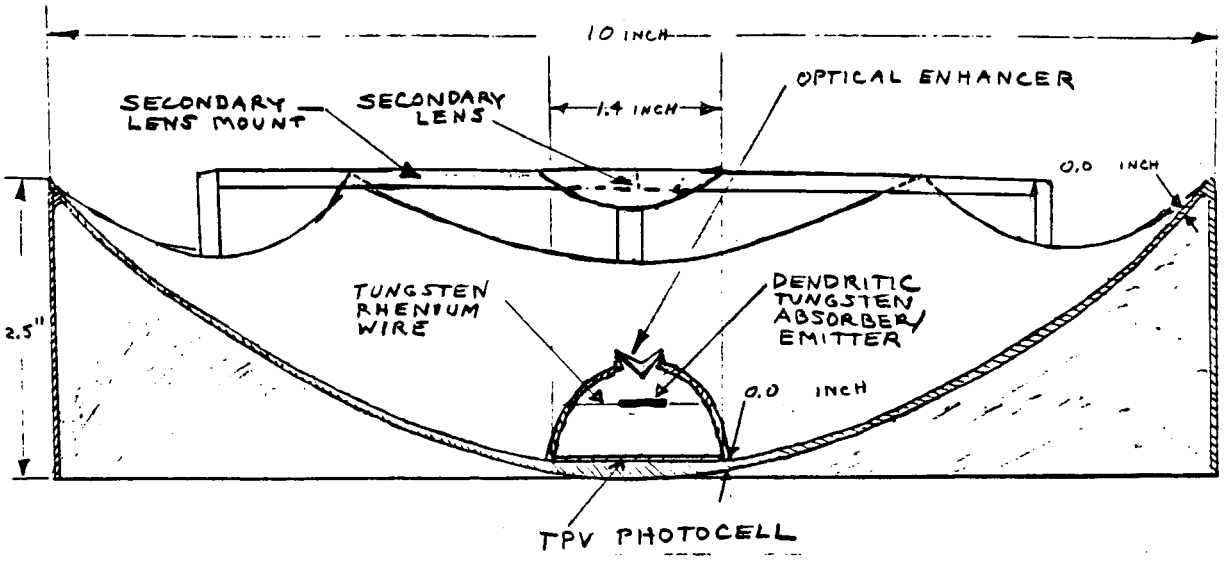

Figure 11-6. Cross-Sectional View of STPV Module

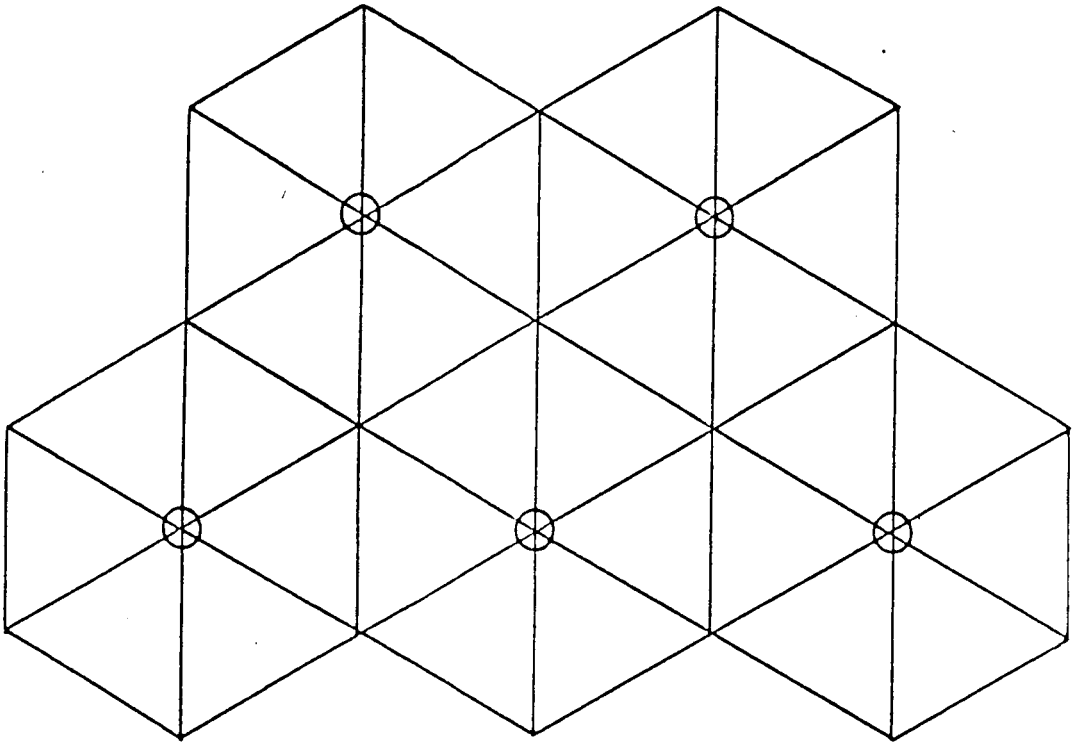

Figure 11-7. Hexagonal TPV Modules Assembled Into a Close-Packed Cluster

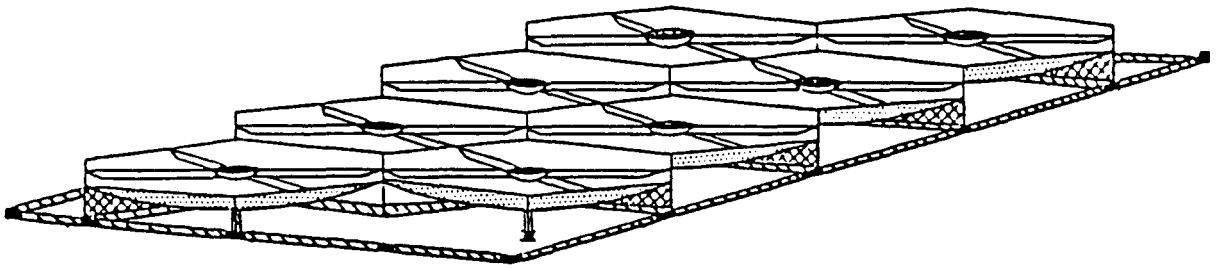

Figure 11-8. TPV Modules Assembled Into a Rigid Panel

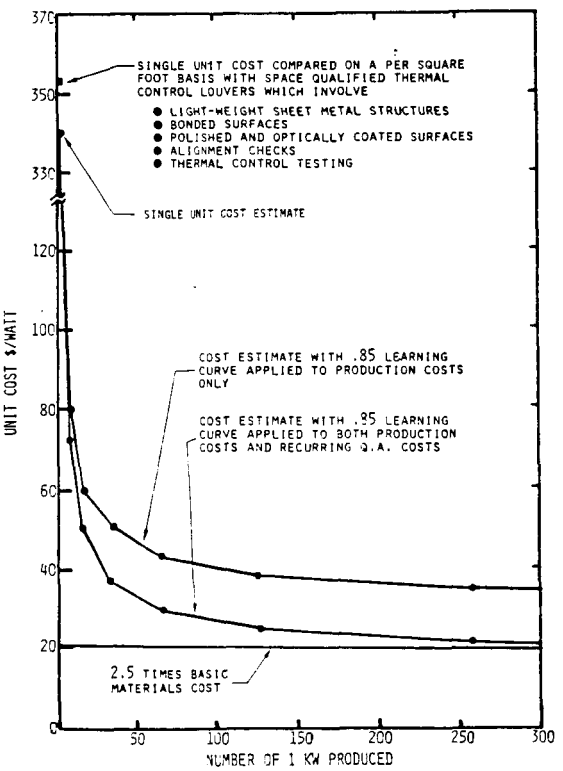

Figure 11-9. Estimated Production Cost Curve for the TPV Modules

12.0 CONCLUSIONS AND RECOMMENDATIONS

From the preceding work, the following conclusions can be drawn:

1. All the engineering questions about STPV feasibility have been addressed both experimentally and analytically and the concept is feasible and operates exactly as expected.

2. A working STPV module has been tested in simulated AMO sunlight and shown to have 12.6% efficiency with off-the-shelf silicon solar cells.

3. A detailed analytical model has been confirmed by the experimental results and predicts efficiencies of 30% with customized cells.

4., A thermal control system has been tested and shown effective for the space environment.

5. A novel optical device has been designed which relieves the pointing tolerances of the STPV to ± 2 degrees.

6. It appears that a new optimized STPV module design will yield 30% efficiency at 300 W/kgm and approximately $20/W in production.

On the basis of these conclusions, it is recommended that a program to develop an optimized TPV photovoltaic cell be implemented.

13.0 REFERENCES

1. "Thermophotovoltaic Space Power System, Phase 3, Interim Report, NAS8-33436, NASA Marshall Space Flight Center, Boeing Document No. D180-27773-1, July 11, 1983.
2. "Study of Silicon and Gallium Arsenide Cells Used in TPV Converter as a Topping Cycle for a Steam Generator," Published by Workers at University of Arkansas, 1978.
3. R. W. Beck and E. H. Sayers, "Study of Germanium Devices for Use in A Thermophotovoltaic Converter," Final Report, Contract DA28-043-AMC-02543(e) (ECOM), General Motors Corporation, November 1967.
4. E. Kittl and G. E. Guazzoni, "Experimental Study of Germanium Cell Performance With Erbium Oxide and Silicon Carbide Radiators," ECOM-3539 Technical Report, Contract 1T6 62705 A 053 01-211, February 1972.
5. E. Kittl and G. Guazzoni, "Designs Analysis of TPV-Generator System," 25th Proceedings Power Sources Conference, May 1972.
6. R. J. Schwartz and N. F. Gardnes, "Theoretical and Experimental Investigation of Planar PIN-Thermophotovoltaic Cells," Final Report, Contract DAAB07-70-C-0129 (ECOM), Purdue University, August 1972.
7. Unpublished Report of System Study Performed by Boeing Space Systems Group.
8. R. M. Swanson and R. N Bracewell, "Silicon Photovoltaic Cells in Thermophotovoltaic Conversion," EPRI ER-478 Progress Report, Research Project 790-1, February 1977.
9. W. E. Horne, "Solar Thermal Photovoltaic Electric Power Generator," Proceedings of Miami International Conference on Alternative Energy Sources, December 1977.
10. M. W. Edinburn, "Systems Analysis of TPV Power Conversion," Unpublished Study Performed by Sandia Laboratories.
11. R. J. Schwartz, N . F. Gardnes, M. Lammert, and P. Munro, "Thermophotovoltaic Cells," Final Report, Contract DAAB07-72-C-0281 (ECOM), Purdue University, June 1974.

12. G. Guazzoni and E. Kittl, "Cylindrical Erbium Oxide Radiator Structures for Thermophotovoltaic Generators," R&D Technical Report ECOM-23259, August 1974.
13. E. Kittl and G. Guazzoni, "Special Studies on Germanium PIN-Photovoltaic Cells for Thermophotovoltaic Conversion," ECOM-4324, Technical Report, Contract 1T2 61102A34A02-311, May 1975.
14. A. Hunt, D. F. Grether, and M. Wahlig, "Circumsolar Radiation Data for Central Receiver Simulation," P. 143, Proceedings of the ERDA Solar Workshop on Methods for Optical Analysis of Central Receiver Systems, Aug. 10-11, 1977, Houston, Texas.